

# Dephasing Enabled Fast Charging of Quantum Batteries

Rahul Shastri,<sup>1</sup> Chao Jiang,<sup>2,3</sup> Guo-Hua Xu,<sup>2</sup> B. Prasanna Venkatesh,<sup>1,\*</sup> and Gentaro Watanabe<sup>2,4,†</sup>

<sup>1</sup>Indian Institute of Technology Gandhinagar, Palaj, Gujarat 382055, India

<sup>2</sup>Department of Physics and Zhejiang Institute of Modern Physics,  
Zhejiang University, Hangzhou, Zhejiang 310027, China

<sup>3</sup>Graduate School of China Academy of Engineering Physics, Beijing 100193, China

<sup>4</sup>Zhejiang Province Key Laboratory of Quantum Technology and Device,  
Zhejiang University, Hangzhou, Zhejiang 310027, China

We propose and analyze a universal method to obtain fast charging of a quantum battery by a driven charger system using controlled, pure dephasing of the charger. While the battery displays coherent underdamped oscillations of energy for weak charger dephasing, the quantum Zeno freezing of the charger energy at high dephasing suppresses the rate of transfer of energy to the battery. Choosing an optimum dephasing rate between the regimes leads to a fast charging of the battery. We illustrate our results with the charger and battery modeled by either two-level systems or harmonic oscillators. Apart from the fast charging, the dephasing also renders the charging performance more robust to detuning between the charger, drive, and battery frequencies for the two-level systems case.

## I. INTRODUCTION

Quantum thermodynamics lies at the intersection of fundamental and applied aspects of quantum technologies. This is evident from the problem statements in the field which are typically structured around microscopic versions of macroscopic machines like heat engines, refrigerators, batteries, etc. While the practical utility of such quantum thermal machines is still nascent, the fundamental aspects uncovered by studying them are expected to influence the design and optimization of current and future quantum devices [1]. In this context, one goal has been to uncover phenomena that are unique or advantageous in quantum thermal machines with no simple counterpart in the classical world [2, 3]. In the specific case of quantum batteries, which are quantum systems that store energy and are charged by direct parametric driving or via ancillary quantum *charger* systems, significant effort has been devoted to identifying situations where figures of merit such as the total energy and ergotropy that can be stored, charging and discharging time, and charging power are optimized [2, 4–10]. Following the seminal work on quantum batteries by Alicki and Fannes [11] showing that entangling unitary protocols can extract more work from identical copies of quantum batteries than independent operation, a key approach to obtain quantum advantage in batteries via collective effects has now emerged [12–23].

While early studies of quantum batteries modeled the charging and discharging processes using closed unitary dynamics, there has been a concerted effort recently to extend this paradigm by including dissipative effects [24–41]. One motivation to include dissipation stems from the recognition that all realistic quantum battery systems

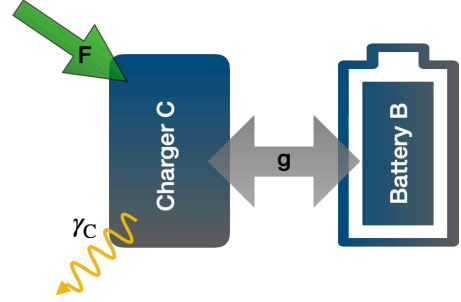


FIG. 1. (Color Online) Schematic of the set-up of a quantum battery B coupled to a quantum charger system C driven at a rate  $F$  and additionally subject to dephasing at the rate  $\gamma_C$ .

will be subject to interactions with their environment and it is imperative to assess and, if possible, mitigate the negative impact of the resulting dissipation on the battery's performance [25–27, 29, 32, 38, 41]. In contrast, viewing dissipation as a resource for state preparation [42–44], a series of works have highlighted the possibility of stable charging using collective dissipation [24, 28, 34], sequential measurements [45], and enhanced energy accumulation via reservoir engineering [40]. Moreover, a small number of works also have pointed out the possibility of achieving higher power and fast charging using dissipative effects [28, 31, 33–37, 39]. However, such demonstrations of charging advantage require restricted settings such as specific models of dissipation [31, 35], collective effects [28, 34, 35, 39], control schemes [36], or particular choices of battery systems [33, 37]. Thus, a simple strategy to obtain fast and stable charging applicable to a wide variety of systems would be highly valuable.

Here, we address this challenge by proposing a universal method to obtain fast charging of a battery by controlled dephasing of the charger. In particular, we consider the scenario of a quantum battery connected to

\* prasanna.b@iitgn.ac.in

† gentaro@zju.edu.cn

a driven quantum charger system that is subject to pure dephasing as shown schematically in Fig. 1. We note that pure dephasing is one of the fundamental decoherence channels for open quantum systems [46] and involves the damping of off-diagonal elements of the density matrix. Most generically, pure dephasing is generated by the coupling of an operator that commutes with the system Hamiltonian, often taken to be the Hamiltonian itself, with the environment. At small values of dephasing, as long as the charger-battery system is initialized in any state apart from the eigenstates of the total Hamiltonian, we expect coherent underdamped oscillation of the battery's energy. In contrast, viewing the pure dephasing process as a continuous measurement of the charger's energy by the environment, strong dephasing naturally leads to a quantum Zeno freezing of the charger's energy and consequent suppression of the rate of charging of the battery. Thus for any charger and battery system, at an in-between moderate value of dephasing that provides a balance between the two effects, we should see an optimum fast charging of the battery. This is akin to the working of a shock absorber in a car where adding a dissipative element with the appropriate amount of damping ensures a smooth transfer of mechanical impulse. The wide applicability of our strategy is further strengthened by the fact that pure dephasing is a ubiquitous source of dissipation in a variety of quantum systems like superconducting qubits, NMR, and trapped ions naturally generated by energy-conserving coupling of the system to noisy external electromagnetic fields [47–49]. We confirm and illustrate our general strategy of dephasing-enabled fast charging by choosing the battery and charger systems as two-level systems (TLS) and quantum harmonic oscillators (HO). Moreover, we also find that the dephased charger also lends a certain degree of robustness to the charging process. In particular, we find that for the TLS case, the charging energy for a detuned driving of the battery is larger in the dephased case compared to the closed system for a wide range of driving frequencies shifted from the resonance.

The article is structured as follows. In Sec. II, we introduce the general setup of a charger-mediated quantum battery followed by a description of the specific examples of the two-level system and quantum harmonic oscillator battery and charger. Following this, we present our central results in Sec. III with the results for the TLS in Sec. III A and the HO in Sec. III B. We conclude in Sec. IV by summarizing our findings and identifying promising experimental systems where our central idea can be implemented. We present additional details in Appendices A, B, and C.

## II. MODEL AND SET-UP

We consider a charger-mediated quantum battery setup consisting of a charger system C, and a quantum battery B. The Hamiltonian of the total system has the

following general form

$$\hat{H}(t) = \hat{H}_C + \hat{H}_d(t) + \hat{H}_B + \hat{H}_{CB}, \quad (1)$$

where  $\hat{H}_C$  and  $\hat{H}_B$  are the bare Hamiltonians of the charger and battery system respectively,  $\hat{H}_d$  denotes the coherent driving of the charger system that is the energy source, and  $\hat{H}_{CB}$  is the coupling Hamiltonian between the charger and battery that enables the charging process. In addition to the unitary dynamics generated by  $\hat{H}$ , the charger system undergoes a pure dephasing process that will be described via a Gorini-Kossakowski-Sudarshan-Lindblad (GKLS) master equation with a hermitian jump operator  $\hat{L}_C$  that satisfies  $[\hat{L}_C, \hat{H}_C] = 0$ . Thus the time evolution of the density matrix  $\hat{\rho}$  describing the charger and battery system is given by

$$\frac{d\hat{\rho}(t)}{dt} = -i [\hat{H}, \hat{\rho}(t)] + \gamma_C \left( \hat{L}_C \hat{\rho}(t) \hat{L}_C - \frac{\{\hat{L}_C^2, \hat{\rho}(t)\}}{2} \right), \quad (2)$$

with  $\gamma_C$  giving the rate of dephasing and  $\{\cdot, \cdot\}$  denoting the anticommutator. Taking the jump operator as  $\hat{L}_C \propto \hat{H}_C$ , allows the interpretation of the pure dephasing process in Eq. (2) as resulting from a continuous weak measurement of the energy [50] of the charger system. Starting with the charger and battery system in their respective (free) ground states, the evolution generated by Eq. (2) leads to an increase in the energy and ergotropy of the battery system that is defined as

$$E_B = \text{Tr}_B [\hat{\rho}_B \hat{H}_B], \quad (3)$$

$$\mathcal{E}_B = E_B - \min_{\hat{U}_B} \text{Tr}_B [\hat{U}_B \hat{\rho}_B \hat{U}_B^\dagger \hat{H}_B], \quad (4)$$

respectively. Here  $\hat{\rho}_B \equiv \text{Tr}_C [\hat{\rho}]$  ( $\hat{\rho}_C \equiv \text{Tr}_B [\hat{\rho}]$ ) is the reduced density matrix of the battery (charger) and in Eq. (4) the minimization is performed over all possible unitaries  $\hat{U}_B$  in the battery's Hilbert space. Apart from the values of energy and ergotropy that serve as the standard figures of merit to describe the charging performance, we are specifically interested in the charging time of the battery. As we will describe this in detail with specific systems below, the charging time can be sensibly defined in cases where the battery goes to the steady state under the combined action of the drive and dephasing of the charger.

To illustrate our central results regarding the charging advantages with a dephased charger, we will consider the charger and battery to be given by a two-level system and the harmonic oscillator. Our choice is motivated by the fact that the TLS and HO represent two extremes as far as energy spectrum of quantum systems are concerned. They are indeed the simplest examples of non-linear bounded and linear (equispaced) unbounded energy spectrum. Moreover, they are canonical systems in quantum optics and are readily realizable in various

experiments. In the scenario where both the charger and battery are TLSs, the Hamiltonian is given by

$$\hat{H} = \omega_C \hat{\sigma}_C^+ \hat{\sigma}_C^- + \omega_B \hat{\sigma}_B^+ \hat{\sigma}_B^- + g(\hat{\sigma}_C^+ \hat{\sigma}_B^- + \hat{\sigma}_B^+ \hat{\sigma}_C^-) + F(\hat{\sigma}_C^- e^{i\omega_d t} + \hat{\sigma}_C^+ e^{-i\omega_d t}), \quad (5)$$

with  $\hat{\sigma}_B^+ = \hat{\sigma}_B^-^\dagger$ ,  $\hat{\sigma}_C^+ = \hat{\sigma}_C^-^\dagger$  representing the Pauli raising operators for the battery and charger,  $\omega_B$  ( $\omega_C$ ) giving the frequency of the battery (charger), and  $F$ ,  $\omega_d$  denoting the driving strength and frequency of the charger. In addition, the jump operator that gives the pure dephasing in Eq. (1) for TLS is given by  $\hat{L}_C = \hat{\sigma}_C^+ \hat{\sigma}_C^- = (\hat{\sigma}_C^z + \mathcal{I})/2$ . Along the same lines, for the HO charger and battery, the Hamiltonian is given by

$$\hat{H} = \omega_C \hat{a}_C^\dagger \hat{a}_C + \omega_B \hat{a}_B^\dagger \hat{a}_B + g(\hat{a}_C^\dagger \hat{a}_B + \hat{a}_B^\dagger \hat{a}_C) + F(\hat{a}_C e^{i\omega_d t} + \hat{a}_C^\dagger e^{-i\omega_d t}), \quad (6)$$

with  $\hat{a}_B$  and  $\hat{a}_C$  denoting the annihilation operators for the battery and charger HO respectively, and the jump operator for the charger dephasing is given by  $\hat{L}_C = \hat{a}_C^\dagger \hat{a}_C$ . Note that in both the TLS and HO case, the choice of the coupling is such that  $[\hat{H}_C + \hat{H}_B, \hat{H}_{CB}] = 0$  ensuring that there is no energetic cost to switch on/off the interaction in the absence of the charger driving with the battery and charger at resonance.

### III. RESULTS

In this section, we present our central results by considering specific realizations of the charger-battery system consisting of TLSs and HOs. We begin by considering the scenario with both charger and battery given by TLSs and follow it up with the case of HOs.

#### A. Two-TLS Model

To simplify the analysis for the TLS case, it is convenient to move to an interaction picture with respect to the bare Hamiltonians of the charger and battery by considering a unitary transformation  $\hat{U}_{CB} = \exp(-i[\omega_C \hat{\sigma}_C^+ \hat{\sigma}_C^- + \omega_B \hat{\sigma}_B^+ \hat{\sigma}_B^-]t)$  resulting in the following Hamiltonian

$$\hat{H}' = g(\hat{\sigma}_C^+ \hat{\sigma}_B^- e^{i\Delta_{CB}t} + \hat{\sigma}_C^- \hat{\sigma}_B^+ e^{-i\Delta_{CB}t}) + F(\hat{\sigma}_C^- e^{-i\Delta_{Cd}t} + \hat{\sigma}_C^+ e^{i\Delta_{Cd}t}), \quad (7)$$

with the frequency differences  $\Delta_{CB} = \omega_C - \omega_B$  and  $\Delta_{Cd} = \omega_C - \omega_d$ . Since the jump operator  $\hat{L}_C = \hat{\sigma}_C^+ \hat{\sigma}_C^-$  is invariant under this unitary, the master equation (2) in the interaction picture reads

$$\frac{d\hat{\rho}'(t)}{dt} = -i[\hat{H}', \hat{\rho}'(t)] + \frac{\gamma_C}{4}(\hat{\sigma}_C^z \hat{\rho}'(t) \hat{\sigma}_C^z - \hat{\rho}'(t)), \quad (8)$$

with  $\hat{\rho}' = \hat{U}_{CB}^\dagger \hat{\rho} \hat{U}_{CB}$ . Moreover, for the TLS case, the figures of merit given by energy and ergotropy can be expressed as

$$E_B = \frac{\omega_B}{2} (\langle \hat{\sigma}_B^z \rangle + 1), \quad (9)$$

$$\mathcal{E}_B = \frac{\omega_B}{2} \left( \sqrt{\langle \hat{\sigma}_B^z \rangle^2 + 4\langle \hat{\sigma}_B^+ \rangle \langle \hat{\sigma}_B^- \rangle} + \langle \hat{\sigma}_B^z \rangle \right). \quad (10)$$

in terms of the first moments of the battery operators<sup>1</sup>. Since the figures of merit depend directly on the moments of the TLS operators, to study the dynamics and properties of energy and ergotropy we can write down a closed set of equations for the moments (first and second) of the TLS operators from the master equation (8) which read as:

$$\begin{aligned} \frac{d}{dt} \langle \hat{\sigma}_B^z \rangle &= -4g\mathfrak{Jm} [e^{i\Delta_{CB}t} \langle \hat{\sigma}_C^+ \hat{\sigma}_B^- \rangle], \\ \frac{d}{dt} \langle \hat{\sigma}_C^z \rangle &= -4F\mathfrak{Jm} [e^{-i\Delta_{Cd}t} \langle \hat{\sigma}_C^- \rangle] \\ &\quad + 4g\mathfrak{Jm} [e^{i\Delta_{CB}t} \langle \hat{\sigma}_C^+ \hat{\sigma}_B^- \rangle], \\ \frac{d}{dt} \langle \hat{\sigma}_C^+ \hat{\sigma}_B^- \rangle &= -iF e^{-i\Delta_{Cd}t} \langle \hat{\sigma}_C^z \hat{\sigma}_B^- \rangle - \frac{\gamma_C}{2} \langle \hat{\sigma}_C^+ \hat{\sigma}_B^- \rangle \\ &\quad - i\frac{g}{2} e^{-i\Delta_{CB}t} (\langle \hat{\sigma}_C^z \rangle - \langle \hat{\sigma}_B^z \rangle), \\ \frac{d}{dt} \langle \hat{\sigma}_C^z \hat{\sigma}_B^- \rangle &= -2iF (e^{i\Delta_{Cd}t} \langle \hat{\sigma}_C^+ \hat{\sigma}_B^- \rangle - e^{-i\Delta_{Cd}t} \langle \hat{\sigma}_C^- \hat{\sigma}_B^- \rangle) \\ &\quad + i g e^{-i\Delta_{CB}t} \langle \hat{\sigma}_C^- \rangle, \\ \frac{d}{dt} \langle \hat{\sigma}_C^- \hat{\sigma}_B^- \rangle &= iF e^{i\Delta_{Cd}t} \langle \hat{\sigma}_C^z \hat{\sigma}_B^- \rangle - \frac{\gamma_C}{2} \langle \hat{\sigma}_C^- \hat{\sigma}_B^- \rangle, \\ \frac{d}{dt} \langle \hat{\sigma}_C^- \rangle &= iF e^{i\Delta_{Cd}t} \langle \hat{\sigma}_C^z \rangle + i g e^{i\Delta_{CB}t} \langle \hat{\sigma}_C^z \hat{\sigma}_B^- \rangle \\ &\quad - \frac{\gamma_C}{2} \langle \hat{\sigma}_C^- \rangle, \end{aligned} \quad (11)$$

and

$$\begin{aligned} \frac{d}{dt} \langle \hat{\sigma}_B^- \rangle &= i g e^{-i\Delta_{CB}t} \langle \hat{\sigma}_C^- \hat{\sigma}_B^z \rangle, \\ \frac{d}{dt} \langle \hat{\sigma}_C^- \hat{\sigma}_B^z \rangle &= iF e^{i\Delta_{Cd}t} \langle \hat{\sigma}_C^z \hat{\sigma}_B^z \rangle + i g e^{i\Delta_{CB}t} \langle \hat{\sigma}_B^- \rangle \\ &\quad - \frac{\gamma_C}{2} \langle \hat{\sigma}_C^- \hat{\sigma}_B^z \rangle, \\ \frac{d}{dt} \langle \hat{\sigma}_C^z \hat{\sigma}_B^z \rangle &= -4F\mathfrak{Jm} [e^{-i\Delta_{Cd}t} \langle \hat{\sigma}_C^- \hat{\sigma}_B^z \rangle]. \end{aligned} \quad (12)$$

Choosing the density matrix at initial time as  $\hat{\rho}'(t=0) = |g\rangle\langle g|_B \otimes |g\rangle\langle g|_C$  with  $|g\rangle_B$  ( $|g\rangle_C$ ) denoting the ground state of the battery (charger), the initial conditions for the moments become:

$$\begin{aligned} \langle \hat{\sigma}_B^z \rangle(0) &= \langle \hat{\sigma}_C^z \rangle(0) = -1, \\ \langle \hat{\sigma}_C^+ \hat{\sigma}_B^- \rangle(0) &= \langle \hat{\sigma}_C^z \hat{\sigma}_B^- \rangle(0) = \langle \hat{\sigma}_C^- \hat{\sigma}_B^- \rangle(0) = \langle \hat{\sigma}_C^- \rangle(0) = 0, \\ \langle \hat{\sigma}_B^- \rangle(0) &= \langle \hat{\sigma}_C^- \hat{\sigma}_B^z \rangle(0) = 0, \\ \langle \hat{\sigma}_C^z \hat{\sigma}_B^z \rangle(0) &= 1. \end{aligned} \quad (13)$$

<sup>1</sup> Note that the average energy and ergotropy remain the same in both the Schrödinger and interaction pictures [27].

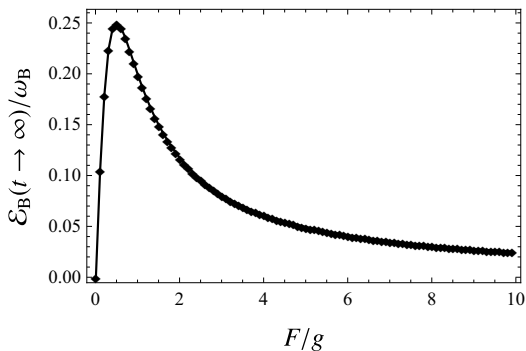


FIG. 2. Asymptotic steady-state values of ergotropy of the battery for the two-TLS model as a function of the ratio between the driving and coupling strength  $F/g$  for the resonant case i.e.  $\omega_C = \omega_d = \omega_B$ .

We begin analysis of the results by considering the resonant case with  $\omega_B = \omega_C = \omega_d$ , i.e.,  $\Delta_{CB} = \Delta_{Cd} = 0$ . We obtain an exact analytical solution for the dynamics corresponding to Eqs. (11) and (12) with the initial conditions Eq. (13). The details of the calculation and the exact expression for the average energy of the battery  $E_B(t)$ , which is cumbersome, is presented in Eq. (A10) of Appendix A 1. Before turning to the analysis of the dynamics, let us consider the energy and ergotropy delivered to the battery in the long-time, steady-state limit which becomes [27] (see Appendix A 1)

$$E_B(t \rightarrow \infty) = \frac{1}{2}, \quad (14)$$

$$\mathcal{E}_B(t \rightarrow \infty) = \frac{\frac{F}{g}}{1 + 4\frac{F^2}{g^2}}. \quad (15)$$

As apparent from the above expression and shown in Fig. 2, the steady state ergotropy is maximized for the optimal value of forcing  $F/g = 0.5$ . The existence of such optimal drive is consistent with previous work reported by Farina *et al.* [27]. Armed with this insight regarding the optimal value of driving, let us now examine the charging dynamics. As mentioned before, the exact analytical solution for the energy and ergotropy enables the following analysis, but since the expressions are cumbersome they are presented in Appendix A 1. To illustrate our central result, we plot the time evolution of the average energy  $E_B$  (a) and ergotropy  $\mathcal{E}_B$  (b) in Fig. 3 for different values of charger dephasing  $\gamma_C$  for precisely the value of the driving  $F/g = 0.5$  that maximizes the steady state ergotropy. As evident from the plot, both ergotropy and average energy display underdamped oscillations for very small  $\gamma_C$  and slow overdamped behavior at very large  $\gamma_C$ . Crucially, at an intermediate optimal value of  $\gamma_C$  where the dynamics transitions from underdamped to overdamped, the ergotropy and average energy reach their steady values in the shortest time. The charging time of the battery, which will be defined in a precise manner soon, is essentially the time taken for the

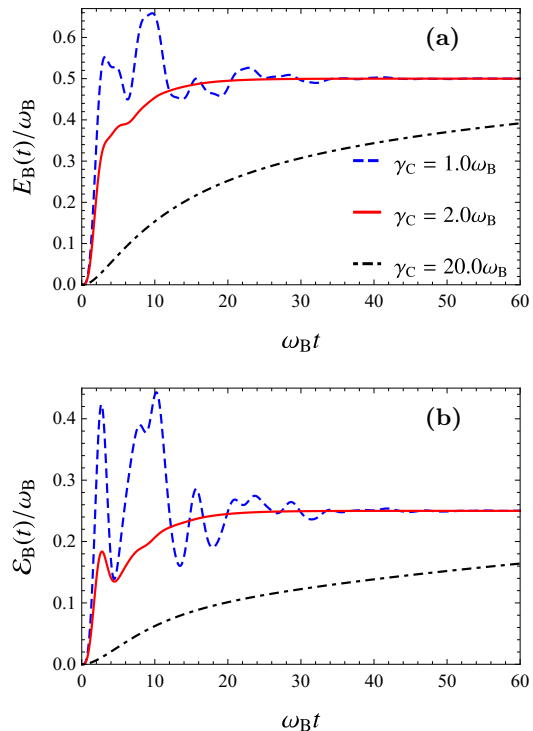


FIG. 3. (Color Online) Time evolution of average energy  $E_B(t)$ (a) and ergotropy  $\mathcal{E}_B(t)$ (b) of the battery for the two-TLS model for the optimal driving case with  $F = 0.5\omega_B, g = 1.0\omega_B$  ( $F/g = 0.5$ ), for different values of the dephasing rate  $\gamma_C$  for the resonant case, i.e.,  $\omega_C = \omega_d = \omega_B$ .

energy (or ergotropy) to approach their steady, long-time values. Thus our main result is that while the charging time is long for both small and large  $\gamma_C$ , a moderate amount of charger dephasing leads to a fast charging of the quantum battery. Before we define and scrutinize the behavior of the charging time and the optimal amount of dephasing that leads to fast charging, we note that our result is general in the sense that both for weak  $F/g \ll 1$  and strong driving  $F/g \gg 1$ , as shown in Figs. 4 and 5 respectively, the dephasing rate for the dynamics of the average energy can be chosen optimally to obtain fast charging. Similar results are applicable for the ergotropy and are displayed in Appendix A 1. A qualitative way to understand this rather general behavior is to first note that in the limit where the dephasing is smaller than the interaction  $\gamma_C < g$ , the persistent oscillatory exchange of energy between the charger and battery, for our choice of the initial state, dies down slowly leading to slow charging. On the other hand, large dephasing  $\gamma_C \gg g$ , leads to the charger energy becoming constant due to the quantum Zeno effect. This naturally suppresses the battery charging leading to very slow transfer of energy to the battery. A moderate dephasing rate provides a trade-off between the two effects, similar to how a shock absorber in an automobile acts as a dissipative element that ensures a smooth transfer of mechanical impulse. Since the exact expression of the energy is more compact in com-

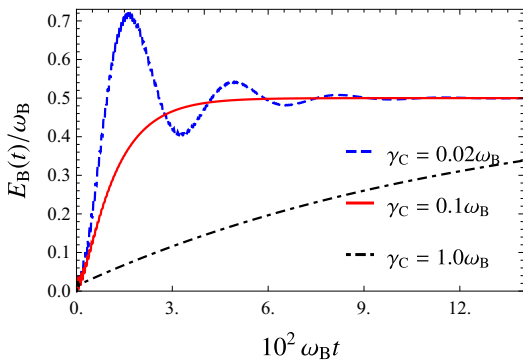


FIG. 4. (Color Online) Time evolution of average energy  $E_B(t)$  of the battery for the two-TLS model for the weak driving case with  $F = 0.1\omega_B, g = \omega_B$  ( $F/g = 0.1$ ), for different values of the dephasing rate  $\gamma_C$  and resonant driving, i.e.,  $\omega_C = \omega_d = \omega_B$

parison to that of the ergotropy and the dynamics of the energy and ergotropy are qualitatively similar, we will use the average energy of the battery for the charging time analysis. As evident from Eq. (A10), the energy as a function of time has an exponential relaxation behavior with the nature of damping (over or under) controlled by the values of damping  $\gamma_C/g$  and driving  $F/g$ . Thus, we define the charging time  $\tau$  for the battery as

$$\left| \frac{E_B(\tau) - E_B(\infty)}{E_B(0) - E_B(\infty)} \right| = e^{-n}, \quad (16)$$

where  $n \geq 1$  is an integer we choose. We calculate  $\tau$  by numerically finding roots of Eq. (16). While the typical choice of  $n = 1$  describes the convergence of the energy to its steady value to one natural logarithm decade, we find that for scenarios with oscillatory terms of higher amplitude, a larger  $n$  gives a smoother variation of charging time as other parameters like the dephasing rate are varied. We would like to clarify that the definition Eq. (16) is not a unique choice for the charging time and provides only one way to estimate this quantity. It is clear that perfect charging to the steady state value only results in the limit of infinite time as we are modeling our dissipation via GKSL master equations. We plot charging time  $\tau$ , calculated from Eq. (16) with  $n = 18$ , as a function of the dephasing rate  $\gamma_C$  in weak Fig. 6(a), strong Fig. 6(b), and intermediate Fig. 6(c) (which maximizes steady state ergotropy) driving strength regimes respectively. In all three regimes we can see that the charging time is minimized at a given optimal value of dephasing, say  $\gamma_C = \gamma_C^*$ , underscoring our central result that moderate dephasing leads to fast charging. We find that taking even larger values of  $n > 18$  will only make the behavior of the charging time in Fig. 6 smoother but not affect any of the important qualitative features, especially the value of  $\gamma_C^*$  (see in particular Fig. 6(c) where the scattering of the data points is still discernible). Exploiting the exact expression for the battery's average energy, we next obtain analytic expressions for the charging time at

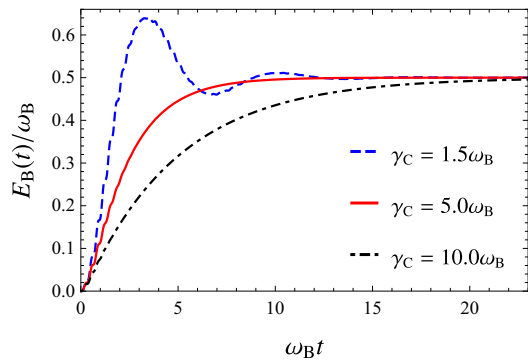


FIG. 5. (Color Online) Time evolution of average energy  $E_B(t)$  of the battery for two-TLS model for the strong driving case  $F = 10.0\omega_B, g = \omega_B$  ( $F/g = 10.0$ ) for different values of the dephasing rate  $\gamma_C$  and resonant driving, i.e.,  $\omega_C = \omega_d = \omega_B$ .

large ( $\gamma_C \gg g$ ) and small dephasing ( $\gamma_C \ll g$ ) regimes. This will allow us to also provide explicit analytical estimates for the optimal dephasing rate  $\gamma_C^*$ . Taking the small dephasing limit ( $\gamma_C \ll g$ ) in the exact expression of the energy, Eq. (16) that determines the charging time takes the form

$$\left| e^{-\frac{\gamma_C}{4}\tau} \phi(F, g, \gamma_C, \tau) \right| = e^{-n}, \quad (17)$$

where the function  $\phi(F, g, \gamma_C, t)$  contains only sinusoidal oscillatory terms [see Eq. (A15) in Appendix A 2 for the detailed expression of  $\phi$ ]. Thus, from Eq. (17), it is evident that the charging time scales as,

$$\tau \sim \frac{4n}{\gamma_C} \quad (18)$$

in the small dephasing limit irrespective of the values of  $F$  and  $g$ . This is neatly illustrated in Figs. 6(a), 6(b), and 6(c), where the behavior of the calculated charging time compares well with the red dashed curve representing the scaling given by Eq. (18) at small  $\gamma_C$ . In the large dephasing limit, to simplify the energy expression we assume  $\gamma_C \gg F$  (in addition to  $\gamma_C \gg g$ ), which consequently leads Eq. (16) to reduce to

$$\frac{1}{2 \left(1 + \frac{4F^2}{g^2}\right)} \left| \frac{8F^2}{g^2} e^{-\frac{2g^2}{\gamma_C}\tau} + \left(1 + \sqrt{1 + \frac{4F^2}{g^2}}\right) e^{-\frac{4f_1 g^2}{\gamma_C}\tau} + \left(1 - \sqrt{1 + \frac{4F^2}{g^2}}\right) e^{-\frac{4f_2 g^2}{\gamma_C}\tau} \right| = e^{-n}, \quad (19)$$

where  $f_1 = 1 + \frac{2F^2}{g^2} - \sqrt{1 + \frac{4F^2}{g^2}}$  and  $f_2 = 1 + \frac{2F^2}{g^2} + \sqrt{1 + \frac{4F^2}{g^2}}$ . In contrast to the small dephasing limit, here we have three damping time scales and the charging time will be decided by the slowest scale among them. As we show in more detail in Appendix A 2, while for the

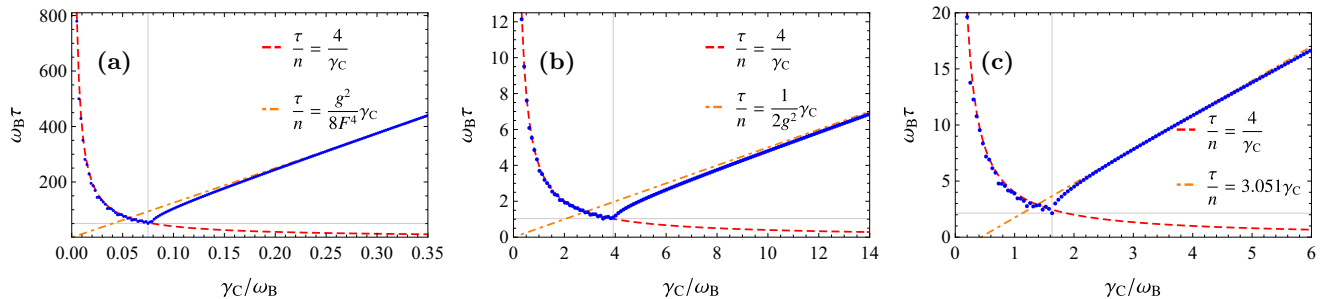


FIG. 6. (Color Online) Charging time of the battery  $\tau$  for the two-TLS model as a function of the charger dephasing rate  $\gamma_C$  for weak driving  $F = 0.1\omega_B, g = \omega_B$  ( $F/g = 0.1$ ) (a), strong driving  $F = 10.0\omega_B, g = \omega_B$  ( $F/g = 10.0$ ) (b), and optimal driving  $F = 0.5\omega_B, g = \omega_B$  ( $F/g = 0.5$ ) (c) for the resonant case, i.e.,  $\omega_C = \omega_d = \omega_B$ . Gray vertical lines indicate the value,  $\gamma_C^*$ , of the optimal dephasing to get the fastest charging time.

weak driving  $F/g \ll 1$  regime the slowest damping scale comes from the second term ( $4f_1/\gamma_C$ ), in the strong driving  $F/g \gg 1$  it is given by the first term ( $2/\gamma_C$ ). This allows us to determine the scaling of the charging time at large damping as

$$\tau \sim \frac{ng^2}{F^4} \gamma_C \text{ for } F/g \ll 1 \quad (20)$$

$$\tau \sim \frac{n}{2g^2} \gamma_C \text{ for } F/g \gg 1. \quad (21)$$

This large dephasing scaling is clearly illustrated by the orange dash-dotted lines in Fig. 6(a) for the weak driving  $F/g \ll 1$  and Fig. 6(b) for the strong driving  $F/g \gg 1$ . From the damping exponentials in Eq. (19), it is clear that the charging time should scale linearly with the dephasing rate for all values of  $F/g$ . However, in the intermediate, moderate regime for the ratio of the driving to the coupling strength with  $F \sim g$ , we have not been able to determine the analytical form of the pre-factor in the linear scaling of the charging time. In Fig. 6(c), where we plot the charging time as a function of dephasing rate for the optimum driving case with  $F/g = 0.5$ , we have shown the linear behavior at large  $\gamma_C$  with a numerical fit (orange dash-dotted line).

The optimum dephasing rate  $\gamma_C^*$  that leads to the fastest charging lies precisely in between the distinct scaling behaviors we have uncovered above for large and small  $\gamma_C$ . We can perform a quick estimate of  $\gamma_C^*$  by equating the charging time in the small  $\gamma_C$  limit Eq. (18) to the ones in the large  $\gamma_C$  case given in Eqs. (20) and (21). In this manner we obtain

$$\gamma_C^* \stackrel{F \ll g}{\approx} \frac{8F^2}{\sqrt{2}g}, \quad (22)$$

$$\gamma_C^* \stackrel{F \gg g}{\approx} 2\sqrt{2}g, \quad (23)$$

for small and large driving  $F/g$ . As evident from the intersection of the scaling curves in Fig. 6,  $\gamma_C^*$  from this approach is generally lower than the actual optimum. A more accurate value for the optimum dephasing rate

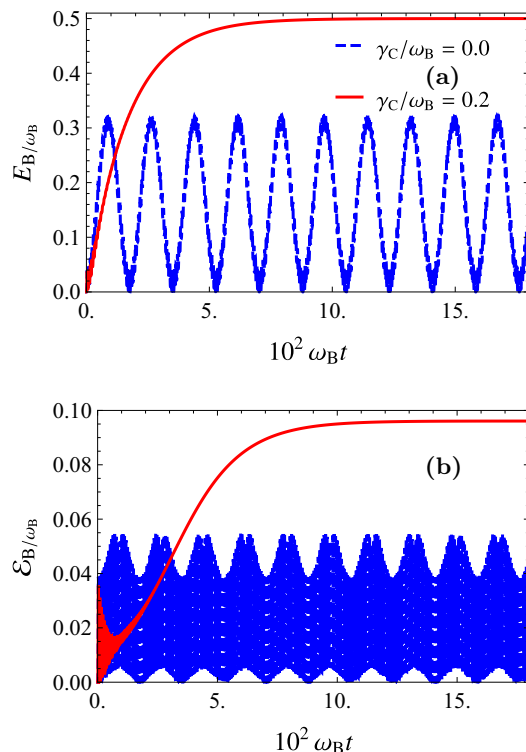


FIG. 7. Transient dynamics of the average energy  $E_B(t)$  [(a)] and ergotropy  $\mathcal{E}_B(t)$  [(b)] of the battery in the weak driving regime  $F/g = 0.1$  for the detuned driving case with  $\Delta_{Cd} = \Delta_{Bd} = 0.015\omega_B$ . Other parameter values are  $g = \omega_B$ .

$\gamma_C^*$  is provided by determining the value of  $\gamma_C$  for which the average energy's dynamics shows an underdamped to overdamped transition. We do this in Appendix A 2 and find qualitatively similar results to Eqs. (22) and (23). Note that one can also define the fastest charging time  $\tau^* \equiv 4/\gamma_C^*$  and it takes the value  $\tau^* \approx 4\sqrt{2}g/(8F^2)$  and  $\tau^* \approx \sqrt{2}/g$  for weak and strong driving respectively.

Let us now consider the charging behavior when the driving or charger is not resonant with the battery. In this case, since the analytical solutions to the equations

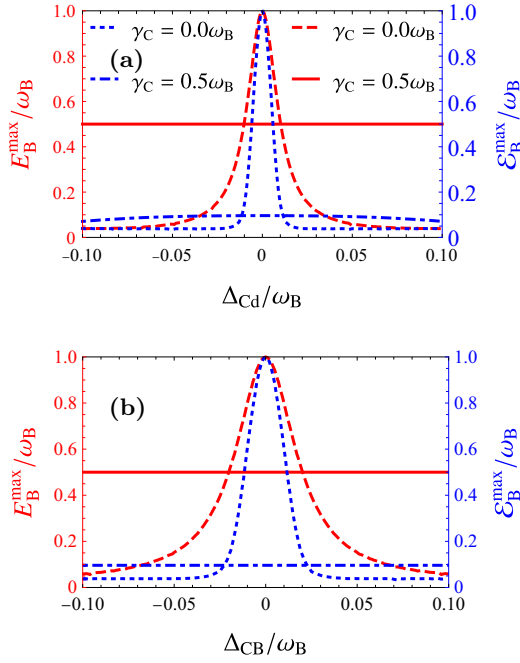


FIG. 8. (Color Online) Maximum value of ergotropy and average energy as a function of drive-battery detuning (a) and charger-battery detuning (b). The long-dashed and solid red lines (left y-axis) and the small-dashed and dash-dotted blue lines (right y-axis) represent the maximum energy and ergotropy respectively. Other parameters are  $F = 0.1\omega_B$  and  $g = 1.0\omega_B$ .

of motion (11) and (12) lead to cumbersome expressions that do not add insight, we stick to depicting the solutions for some exemplary parameter choices. Along this line, we show the transient dynamics of the average energy  $E_B(t)$  in Fig. 7(a) and ergotropy  $\mathcal{E}_B(t)$  in Fig. 7(b) of the battery in the weak driving regime  $F/g = 0.1$  for the case where the driving frequency is detuned from the battery and charger frequency, i.e.,  $\Delta_{Cd} = \Delta_{Bd} \neq 0$ . We see that for the closed ( $\gamma_C = 0$ ) case the average energy and ergotropy of the battery oscillate without damping in Fig. 7. In contrast, for the non-zero dephasing case, as we discuss in detail in Appendix A 3, the energy attains the value  $\omega_B/2$  and the ergotropy goes to zero in the steady-state ( $t \rightarrow \infty$ ) limit. Nonetheless, from Fig. 7 we can readily see that the battery energy and ergotropy take values well above the oscillating closed-case values over a range of time scales. Moreover, for the ergotropy, remarkably, this quasi-steady value persists for a very long time. In this sense, since both the transient maximum of the average energy ( $E_B^{\max}$ ) and ergotropy ( $\mathcal{E}_B^{\max}$ ) for large enough detuning take higher values for the dephased case than in the closed case, we conclude that dephasing provides a degree of robustness against detuning in terms of charging performance. This robustness is summarized in Fig. 8(a), where we plot  $E_B^{\max}$  and  $\mathcal{E}_B^{\max}$  as a function of drive-battery detuning  $\Delta_{Cd}$ . Thus, for a broad range of detuning values, the dephased charging process

attains a higher charging energy compared to the closed case. Moreover, as shown in Fig. 8(b), we find that the same result also holds good for the case where the battery and charger system is detuned but the charger drive is resonant with the battery, i.e.,  $\Delta_{CB} \neq 0, \Delta_{Bd} = 0$ . A point of difference, as we discuss in Appendix A 3, in this case in the long time limit the ergotropy goes to the same steady state non-zero value as the resonant case. We find that the robustness to detuning shown here for weak driving  $F/g \ll 1$  is also present for large values of the ratio between the driving and coupling strength  $F/g \gg 1$ .

In summary, we have demonstrated the advantages of a dephased charger setup for the TLS battery. Our result provides a strategy for the most advantageous way to charge a TLS battery with a charger. To that end, we have to first take the ratio between the driving and coupling strength  $F/g = 0.5$  to obtain the largest steady-state ergotropy of  $\mathcal{E}_B(t \rightarrow \infty) = 0.25\omega_B$ . To obtain the fastest charging time, notice from Fig. 6(c) that the optimal dephasing for the moderate driving regime of  $F/g = 0.5$  is given by  $\gamma_C^* \approx 1.15\omega_B = 2.3F$ . Since the charging time scales inversely with  $\gamma_C^*$ , we can further get the fastest charging by applying the optimum dephasing  $\gamma_C^*$  with the largest allowed value of  $F$  in the particular physical realization. Moreover, in the presence of dephasing, the charging performance is more robust to detuning between the charger and driving than the closed set-up. Finally, we note that the ratio of the maximum steady state ergotropy to total energy, which takes the value of 0.5 in the single TLS battery case above, can be readily increased by considering the scenario where a single central charger interacts with a collection of  $N$  TLS batteries in a star topology [51]. As we demonstrate briefly in Appendix A 1, in this configuration the ratio can be increased to 0.62, 0.69 for  $N = 2, 3$  respectively. We will consider such a set-up with multiple batteries in more detail in a forthcoming work [52].

## B. Two-Harmonic-Oscillator Model

We now consider a set-up with both the charger and battery consisting of quantum harmonic oscillators (HOs). What follows will both reinforce the generality of our central result regarding moderate dephasing leading to fast charging as well as highlight some expected but important differences between the HO and TLS systems. Similar to the TLS case, we first transform to an interaction picture with respect to the bare Hamiltonians of the charger and battery with the unitary transformation  $\hat{U}_{CB} = \exp(-i[\omega_C \hat{a}_C^\dagger \hat{a}_C + \omega_B \hat{a}_B^\dagger \hat{a}_B]t)$  applied on the bare Hamiltonian given by Eq. (6) resulting in the following Hamiltonian

$$\begin{aligned} \hat{H}' = & g \left( \hat{a}_C^\dagger \hat{a}_B e^{i\Delta_{CB}t} + \hat{a}_B^\dagger \hat{a}_C e^{-i\Delta_{CB}t} \right) \\ & + F \left( \hat{a}_C e^{-i\Delta_{Cd}t} + \hat{a}_C^\dagger e^{i\Delta_{Cd}t} \right), \end{aligned} \quad (24)$$

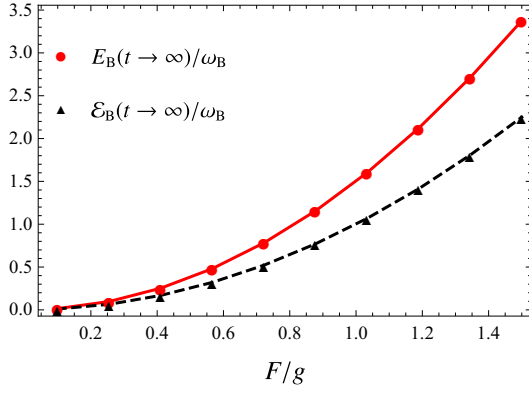


FIG. 9. (Color Online) Asymptotic steady-state values of average energy  $E_B(\infty)$  and ergotropy  $\mathcal{E}_B(\infty)$  of the battery for two Harmonic-Oscillator model as a function of the ratio between the driving and coupling strength  $F/g$  for non-zero charger dephasing rate  $\gamma_C$ . Here solid red line represents the analytical values, and the dashed black line is the fitted values  $(F/g)^2$  to  $\mathcal{E}_B(\infty)$ .

with the detunings defined as in the TLS case. As before, since the jump operator  $\hat{L}_C = \hat{a}_C^\dagger \hat{a}_C$  is invariant under the unitary, the time-evolution generated by Eq. (2) is modified to

$$\begin{aligned} \frac{d\hat{\rho}'(t)}{dt} = & -i \left[ \hat{H}', \hat{\rho}'(t) \right] \\ & + \frac{\gamma_C}{2} \left( \hat{a}_C^\dagger \hat{a}_C \hat{\rho}'(t) \hat{a}_C^\dagger \hat{a}_C - \frac{\{(\hat{a}_C^\dagger \hat{a}_C)^2, \hat{\rho}'(t)\}}{2} \right), \end{aligned} \quad (25)$$

with  $\hat{\rho}' = \hat{U}_{CB}^\dagger \hat{\rho} \hat{U}_{CB}$ . While the total energy stored in the battery can be written as

$$E_B(t) = \omega_B \langle \hat{a}_B^\dagger \hat{a}_B \rangle = \omega_B \text{Tr}_{BC} \left[ \hat{\rho}'(t) \hat{a}_B^\dagger \hat{a}_B \right], \quad (26)$$

for arbitrary (possibly non-Gaussian) quantum states of the battery, a closed-form expression for the ergotropy in terms of expectations of battery operators is not derivable [27, 53]. Indeed in contrast to the work of [27], where the dissipative evolution was Gaussian, the dephasing jump operator generates non-Gaussian states of the oscillators [53]. Thus, we need to resort to numerical solutions of the master equation to compute the ergotropy. Such numerical simulations in general will involve a cut-off in the number of oscillator eigenstates and the required number of states to capture the dynamics faithfully will increase with the ratio between the driving and coupling strength  $F/g$ . Interestingly, as we discuss next in the oscillator case, there is no qualitative distinction in the dynamics for different values of the ratio between the driving and coupling strength  $F/g$  in the sense of its dependence on the charger dephasing rate  $\gamma_C$ . Moreover, we will show that there is a simple scaling relation connecting the dynamics for different  $F/g$ .

Let us, as before, first focus on the resonant case with  $\Delta_{CB} = \Delta_{Cd} = 0$ . We now perform an additional unitary

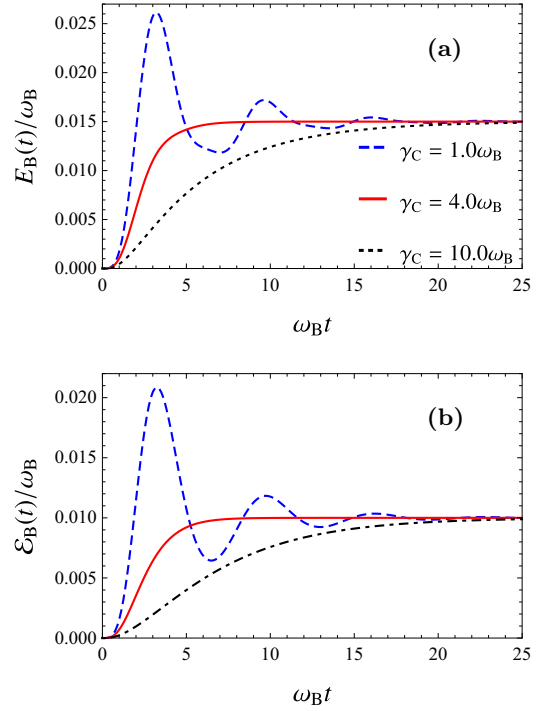


FIG. 10. (Color Online) Time Evolution of average energy  $E_B(t)$ (a) and ergotropy  $\mathcal{E}_B(t)$ (b) of the battery for two Harmonic-Oscillator model in weak driving  $F/g = 0.1$  regimes for different values of the dephasing rate  $\gamma_C$ . Other parameter values are  $g = 1.0\omega_B$ , and  $\omega_C = \omega_d = \omega_B$ .

transformation generated by the displacement operator  $\hat{U} = \hat{D}(F/g) = \exp[F/g(\hat{a}_B^\dagger + \hat{a}_B)]$  which leads to the following master equation for the transformed density operator  $\hat{\rho} = \hat{U} \hat{\rho}' \hat{U}^\dagger$

$$\begin{aligned} \frac{d\hat{\rho}}{dt} = & -i \left[ g \left( \hat{a}_C^\dagger \hat{a}_B + \hat{a}_C \hat{a}_B^\dagger \right), \hat{\rho}(t) \right] \\ & + \gamma_C \left( \hat{a}_C^\dagger \hat{a}_C \hat{\rho}(t) \hat{a}_C^\dagger \hat{a}_C - \frac{1}{2} \left\{ \hat{a}_C^\dagger \hat{a}_C, \hat{\rho}(t) \right\} \right). \end{aligned} \quad (27)$$

where we have used the transformation  $\hat{H} = \hat{U} \hat{H}' \hat{U}^\dagger$  with the property  $\hat{D}(\alpha) \hat{a}_B \hat{D}^\dagger(\alpha) = \hat{a}_B - \alpha$  and  $[\hat{D}(F/g), \hat{a}_C^\dagger] = 0$ . From Eq. (27), we can write down the following closed set of EOMs for the moments

$$\begin{aligned} \frac{d\langle \hat{a}_C \rangle}{dt} &= -ig \langle \hat{a}_B \rangle - \frac{\gamma_C}{2} \langle \hat{a}_C \rangle \\ \frac{d\langle \hat{a}_B \rangle}{dt} &= -ig \langle \hat{a}_C \rangle \\ \frac{d\langle \hat{a}_C^\dagger \hat{a}_C \rangle}{dt} &= 2g \Im \left[ \langle \hat{a}_C^\dagger \hat{a}_B \rangle \right] \\ \frac{d\langle \hat{a}_C^\dagger \hat{a}_B \rangle}{dt} &= -ig \left( \langle \hat{a}_C^\dagger \hat{a}_C \rangle - \langle \hat{a}_B^\dagger \hat{a}_B \rangle \right) - \frac{\gamma_C}{2} \langle \hat{a}_C^\dagger \hat{a}_B \rangle \\ \frac{d\langle \hat{a}_B^\dagger \hat{a}_B \rangle}{dt} &= -2g \Im \left[ \langle \hat{a}_C^\dagger \hat{a}_B \rangle \right], \end{aligned} \quad (28)$$

where the expectation values should be understood as taken with respect to the transformed density operator,

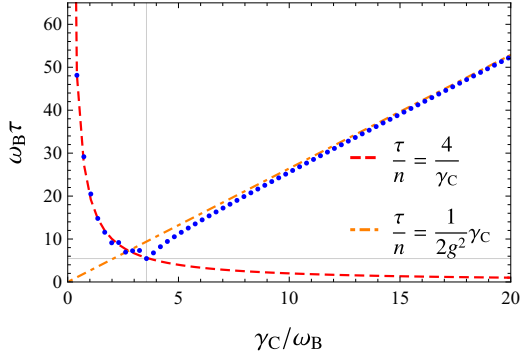


FIG. 11. (Color Online) Charging time  $\tau$  as a function of the dephasing rate of the charger  $\gamma_C$  for the two-HO model of quantum battery in strong and weak driving regimes. Here the red dashed corresponds to fitting Eq. (32), and the orange dashed line is the fitting Eq. (34). The grey vertical line indicates the optimal value,  $\gamma_C^*$ , to obtain faster charging time. Other parameter values are the same as Fig. 10.

i.e.,  $\langle \cdot \rangle = \text{Tr}_{\text{BC}} [\hat{\rho} \cdot]$ . This holds for the initial conditions as well with the initial state  $\hat{\rho}'(0) = |\psi_0\rangle\langle\psi_0|$  with  $|\psi_0\rangle = |0\rangle_{\text{C}} \otimes |0\rangle_{\text{B}}$  transformed to  $\hat{\rho}(0) = |\tilde{\psi}_0\rangle\langle\tilde{\psi}_0|$  with  $|\tilde{\psi}(0)\rangle = |0\rangle_{\text{C}} \otimes |\alpha = F/g\rangle_{\text{B}}$ . Here  $|\alpha = F/g\rangle_{\text{B}} = \hat{D}(F/g)|0\rangle_{\text{B}}$  is a coherent state of the battery. With this, the initial conditions for solving Eq. (28) becomes  $\langle \hat{a}_{\text{C}} \rangle(0) = \langle \hat{a}_{\text{C}}^\dagger \hat{a}_{\text{C}} \rangle(0) = \langle \hat{a}_{\text{C}}^\dagger \hat{a}_{\text{B}} \rangle(0) = 0$ ,  $\langle \hat{a}_{\text{B}} \rangle(0) = F/g$ , and  $\langle \hat{a}_{\text{B}}^\dagger \hat{a}_{\text{B}} \rangle(0) = F^2/g^2$ . We have now reformulated the dynamics such that all of the dependence on the ratio between the driving and coupling strength  $F/g$  comes via the initial conditions. Solving equations (28) with the above initial condition, we get the average energy of the battery with respect to the density matrix  $\hat{\rho}'$  as  $E_{\text{B}}(t)/\omega_{\text{B}} = \text{Tr}_{\text{BC}} [\hat{\rho}'(t)\hat{a}_{\text{B}}^\dagger \hat{a}_{\text{B}}] = \text{Tr}_{\text{BC}} [\hat{\hat{\rho}}(t)\hat{D}(F/g)\hat{a}_{\text{B}}^\dagger \hat{a}_{\text{B}}\hat{D}^\dagger(F/g)]$  as,

$$\begin{aligned} \frac{E_{\text{B}}(t)}{\omega_{\text{B}}} &= \langle \hat{a}_{\text{B}}^\dagger \hat{a}_{\text{B}} \rangle - \frac{F}{g} \langle \hat{a}_{\text{B}}^\dagger + \hat{a}_{\text{B}} \rangle + \frac{F^2}{g^2} \\ &= \frac{F^2}{g^2} \left\{ \frac{3}{2} - \frac{e^{-\frac{\gamma_C t}{4}}}{2} \left[ 4 \cosh\left(\frac{\Gamma t}{4}\right) + 4 \frac{\gamma_C \sinh\left(\frac{\Gamma t}{4}\right)}{\Gamma} \right. \right. \\ &\quad \left. \left. - \cosh\left(\frac{\sqrt{\Gamma^2 - 3(4g)^2 t}}{4}\right) - \frac{\gamma_C \sinh\left(\frac{\sqrt{\Gamma^2 - 3(4g)^2 t}}{4}\right)}{\sqrt{\Gamma^2 - 3(4g)^2}} \right] \right\}, \end{aligned} \quad (29)$$

with  $\Gamma^2 = \gamma_C^2 - (4g)^2$  (and  $\Gamma$  should be read as a possible complex variable). From the above equation, it is now apparent that the ratio between the driving and coupling strength  $F/g$  simply appears as a quadratic scaling factor for the energy stored in the battery. We have been able to confirm the same scaling behavior (as a function of  $F/g$ ) for the ergotropy from numerical calculations of the dynamics. This is most easily seen from the steady state values of energy ( $E_{\text{B}}(\infty)$ ) and ergotropy ( $\mathcal{E}_{\text{B}}(\infty)$ )

displayed in Fig. 9. From Fig. 9 we see that the numerical calculations of the steady state energy agree with the analytical expectation which can be read off from Eq. (29) as

$$\frac{E_{\text{B}}(\infty)}{\omega_{\text{B}}} = \frac{3 F^2}{2 g^2}, \quad (30)$$

and the steady state ergotropy is fitted perfectly by the expression  $\mathcal{E}_{\text{B}}(\infty)/\omega_{\text{B}} \approx F^2/g^2$ , though we do not have an analytical proof for this dependence. Thus, as evident from Eqs. (29) and (30) that  $F/g$  merely serves as a scale for the energy and ergotropy.

With this insight, let us now examine the energy and ergotropy as a function of  $\gamma_C$ . In Fig. 10, we have plotted the dynamics of energy (a) and ergotropy (b) for three different values of  $\gamma_C$ . In line with the consideration for the TLS, we again see that the charging time takes large values for very small or large values of  $\gamma_C$  with an optimum in between. Thus our central result that a moderate amount of charger dephasing leads to fast charging is valid even for the two HOs set-up. It is evident from Eq. (29) that, in the case of the HO, the charging time  $\tau$  and the optimal dephasing  $\gamma_C^*$  are going to be independent of the ratio between the driving and coupling strength  $F/g$ . As with the TLS case, let us estimate the charging time in the large and small dephasing limits using the condition Eq. (16) with  $n = 1$ . First note that at small dephasing  $\gamma_C/g \ll 1$  we get from Eq. (29) the expression,

$$E_{\text{B}}(t) \approx \frac{3 F^2}{2 g^2} - \frac{1 F^2}{2 g^2} e^{-\frac{\gamma_C t}{4}} (4 \cos gt - \cos 2gt). \quad (31)$$

From this, since there is only one damping scale, the charging time is given by

$$\tau \sim \frac{4}{\gamma_C}. \quad (32)$$

On the other hand, in the limit of large dephasing  $\gamma_C/g \gg 1$  we have,

$$E_{\text{B}}(t) \approx \frac{3 F^2}{2 g^2} - 2 \frac{F^2}{g^2} e^{-\frac{2g^2 t}{\gamma_C}} + \frac{F^2}{2g^2} e^{-\frac{8g^2 t}{\gamma_C}}. \quad (33)$$

We now have two damping time scales and we choose the slower of the two, i.e.,  $\frac{2g^2}{\gamma_C}$  and the charging time is given by

$$\tau \sim \frac{1}{2g^2} \gamma_C. \quad (34)$$

Figure 11 illustrates the charging time calculated from the analytical expression Eq. (29) by using the condition Eq. (16) with  $n = 1$  and also validates the limiting behavior described by Eq. (32) and Eq. (34). Equating the small and large dephasing charging times in Eqs. (32) and (34), we determine the optimal dephasing rate (independent of the ratio between the driving and coupling strength  $F/g$ ) as:

$$\gamma_C^* \approx 2\sqrt{2}g. \quad (35)$$

The fastest charging time in the HO case irrespective of driving is given by  $\tau^* \approx \sqrt{2}/g$ . As we commented before, a more accurate estimate of the optimal dephasing can also be obtained by asking for the values of  $\gamma_C$  at which we get underdamped to overdamped transitions in Eq. (29). There are two such transitions possible, namely when  $\Gamma^2 = 0$  and  $\Gamma^2 - 3(4g)^2 = 0$  which occur for  $\gamma_C = 4g$  and  $\gamma_C = 8g$  respectively. Since we expect the optimal dephasing rate to be controlled by the term with the larger amplitude of oscillation [which are the first two terms in the square bracket in Eq. (29)], we have  $\gamma_C^* = 4g$ . This is a better estimate for the optimal damping in comparison to Eq. (35) as evident from Fig. 11.

In contrast to the TLS case, for the HO when there is detuning, either between the charger and driving or battery, we do not find robustness in charging in the presence of dephasing. For the sake of completeness, we present a detailed analysis of this in Appendix B. In summary, we find that our central result of moderate dephasing leading to faster charging extends to the HO case. While the optimum dephasing rate  $\gamma_C^*$  depends on the charger driving strength and charger-battery coupling in the former, it depends solely on the charger-battery coupling in the latter. Moreover, to emphasize further the generality of our results we show in Appendix C that even for the hybrid scenario with a TLS charger and HO battery, our central result of fast charging with moderate dephasing is applicable.

#### IV. CONCLUSION

Quantum batteries are energy storage devices that are susceptible to environmental dissipation effects. The natural question, then, is whether one can utilize these dissipative processes to enhance the overall performance of quantum batteries. One ubiquitous dissipation mechanism is dephasing in which a quantum system gradually loses coherence. In this paper, we have analyzed a universal method to leverage the dephasing of the charger to get fast, stable, and robust charging of a quantum battery. Our method relies on subjecting the charger to an optimal amount of dephasing that provides the appropriate trade-off between coherent oscillatory dynamics of energy expected at a small dephasing rate and the slow exchange of energy expected from the quantum Zeno effect at a large dephasing rate. We have illustrated our general strategy for specific realizations with the charger and battery systems consisting of two-level systems, harmonic oscillators, or a combination of the two. We have derived analytical results for the dynamics and estimates for the optimum dephasing for both TLS and HO cases. Moreover, for the two-TLS charger-battery set-up, we find that dephasing also provides robustness, in terms of charging energy and ergotropy, to detuning the driving from the charger and battery.

Our theoretical findings can be readily verified in state-

of-the-art quantum technology platforms. For instance, recently experimental implementations of quantum batteries have been achieved with superconducting qubits [54], NMR [51], and organic semiconductor microcavity systems [34]. In all of these realizations, the battery and charger systems are indeed exposed to an environment that can lead to dissipation and decoherence. Moreover, a key feature needed to implement our central idea, namely the ability to control the dephasing strength, has already been demonstrated in the experimental platforms of superconducting qubits [55] and NMR systems [51]. While the manipulation of external magnetic field noise provides the control of dephasing in the former case, a cyclic charging protocol with charger-battery coupling unitaries alternated with open dissipative evolution for a chosen duration enabled the same in the latter. Finally, while we have illustrated our idea for single-component battery and charger systems, an interesting direction for future research [52] is to explore in detail the impact of charger dephasing on the charging of a collective battery [14] and the collective charging of a battery [51]. Among other things, we find that charging a collection of batteries with a single charger in a “star” configuration provides an enhancement of the ratio of the steady-state ergotropy to the total energy for the battery.

#### ACKNOWLEDGMENTS

G.W. was supported by the National Natural Science Foundation of China (Grants No. 12375039 and No. 11975199).

#### Appendix A: Two-TLS Model

In this appendix, we provide additional details pertaining to the two-TLS charger battery system. It turns out that the analytical considerations of the two-TLS model are simplified if we rewrite the EOMs given in the main text in Eq. (11) and Eq. (12) into a time-independent form by the transformations  $\hat{\sigma}_B^- \rightarrow \hat{\sigma}_B^- e^{i(\omega_B - \omega_d)t}$ ,  $\hat{\sigma}_C^- \rightarrow \hat{\sigma}_C^- e^{i(\omega_C - \omega_d)t}$  at the level of the operators resulting in

$$\begin{aligned} \frac{d}{dt} \langle \hat{\sigma}_B^z \rangle &= -4g\mathfrak{Jm} [\langle \hat{\sigma}_C^+ \hat{\sigma}_B^- \rangle], \\ \frac{d}{dt} \langle \hat{\sigma}_C^z \rangle &= -4F\mathfrak{Jm} [\langle \hat{\sigma}_C^- \rangle] + 4g\mathfrak{Jm} [\langle \hat{\sigma}_C^+ \hat{\sigma}_B^- \rangle], \\ \frac{d}{dt} \langle \hat{\sigma}_C^+ \hat{\sigma}_B^- \rangle &= -iF \langle \hat{\sigma}_C^z \hat{\sigma}_B^- \rangle - ig (\langle \hat{\sigma}_C^z \rangle - \langle \hat{\sigma}_B^z \rangle) / 2 \\ &\quad - \left[ \frac{\gamma_C}{2} - i(\Delta_{Cd} - \Delta_{Bd}) \right] \langle \hat{\sigma}_C^+ \hat{\sigma}_B^- \rangle, \\ \frac{d}{dt} \langle \hat{\sigma}_C^z \hat{\sigma}_B^- \rangle &= -2iF (\langle \hat{\sigma}_C^+ \hat{\sigma}_B^- \rangle - \langle \hat{\sigma}_C^- \hat{\sigma}_B^- \rangle) + ig \langle \hat{\sigma}_C^- \rangle \\ &\quad - i\Delta_{Bd} \langle \hat{\sigma}_C^z \hat{\sigma}_B^- \rangle, \\ \frac{d}{dt} \langle \hat{\sigma}_C^- \hat{\sigma}_B^- \rangle &= iF \langle \hat{\sigma}_C^z \hat{\sigma}_B^- \rangle \end{aligned}$$

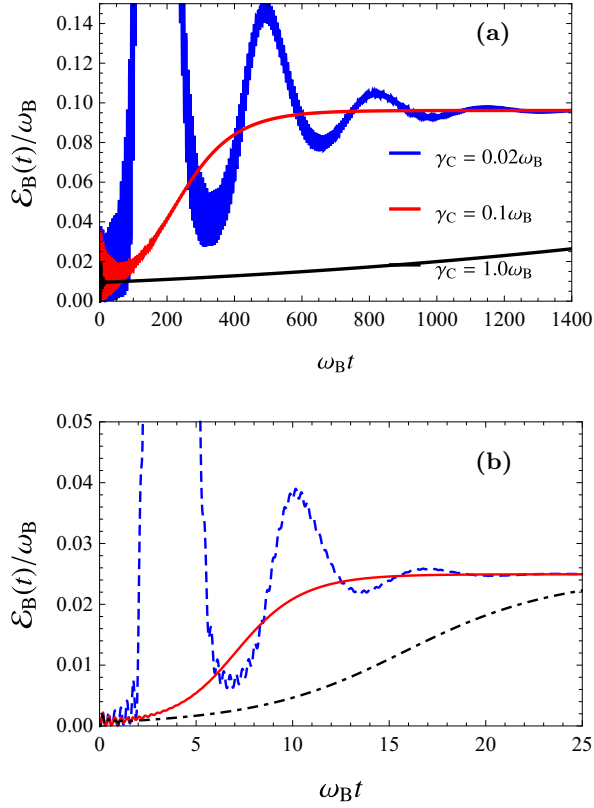


FIG. 12. (Color Online) Time evolution of the ergotropy  $\mathcal{E}_B(t)$  of the battery for two-TLS model for the weak (a) and strong (b) driving case with parameters  $F = 0.1\omega_B, g = \omega_B$  and  $F = 10.0\omega_B, g = \omega_B$  respectively for different values of the dephasing rate  $\gamma_C$ . In both (a) and (b),  $\omega_C = \omega_d = \omega_B$ .

$$\begin{aligned}
 & - \left[ \frac{\gamma_C}{2} + i(\Delta_{Cd} + \Delta_{Bd}) \right] \langle \hat{\sigma}_C^- \hat{\sigma}_B^- \rangle, \\
 \frac{d}{dt} \langle \hat{\sigma}_C^- \rangle &= iF \langle \hat{\sigma}_C^z \rangle + ig \langle \hat{\sigma}_C^z \hat{\sigma}_B^- \rangle - \left( \frac{\gamma_C}{2} + i\Delta_{Cd} \right) \langle \hat{\sigma}_C^- \rangle,
 \end{aligned} \tag{A1}$$

and

$$\begin{aligned}
 \frac{d}{dt} \langle \hat{\sigma}_B^- \rangle &= ig \langle \hat{\sigma}_C^- \hat{\sigma}_B^z \rangle - i\Delta_{Bd} \langle \hat{\sigma}_B^- \rangle, \\
 \frac{d}{dt} \langle \hat{\sigma}_C^- \hat{\sigma}_B^z \rangle &= iF \langle \hat{\sigma}_C^z \hat{\sigma}_B^z \rangle - \left( \frac{\gamma_C}{2} + i\Delta_{Cd} \right) \langle \hat{\sigma}_C^- \hat{\sigma}_B^z \rangle \\
 & \quad + ig \langle \hat{\sigma}_B^- \rangle \\
 \frac{d}{dt} \langle \hat{\sigma}_C^z \hat{\sigma}_B^z \rangle &= -4F \Im [\langle \hat{\sigma}_C^- \hat{\sigma}_B^z \rangle].
 \end{aligned} \tag{A2}$$

Here, as the notation suggests, the detunings  $\Delta_{Cd} = \omega_C - \omega_d$ ,  $\Delta_{Bd} = \omega_B - \omega_d$  are with respect to the driving frequency. The above equations essentially result from a transformation of the original master equation (2) with the unitary  $\hat{U}_d = \exp(-i\omega_d[\hat{\sigma}_C^+ \hat{\sigma}_C^- + \hat{\sigma}_B^+ \hat{\sigma}_B^-]t)$  instead of the transformation to the interaction picture employed in the main text. In this frame rotating with the drive

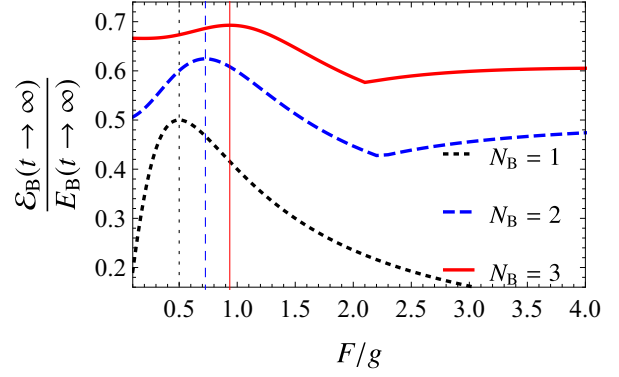


FIG. 13. (Color Online) Asymptotic steady-state values of ergotropy of  $N$  TLS batteries in a star configuration coupled to a single driven TLS charger system as a function of driving strength  $F/g$  for the resonant case, i.e.  $\omega_C = \omega_d = \omega_B$

frequency, the Hamiltonian reads:

$$\begin{aligned}
 \bar{\hat{H}} &= \Delta_{Cd} \hat{\sigma}_C^+ \hat{\sigma}_C^- + \Delta_{Bd} \hat{\sigma}_B^+ \hat{\sigma}_B^- + g (\hat{\sigma}_C^+ \hat{\sigma}_B^- + \hat{\sigma}_C^- \hat{\sigma}_B^+) \\
 & \quad + F(\hat{\sigma}_C^+ + \hat{\sigma}_C^-).
 \end{aligned} \tag{A3}$$

After breaking up the complex expectation values like  $\langle \hat{\sigma}_C^- \rangle$  into their real and imaginary parts, Eqs. (A1) and (A2) reduce to simple homogeneous systems of first order ODEs with time-independent coefficients of the succinct form:

$$\frac{d\vec{V}_1(t)}{dt} = \mathbf{M}_1 \vec{V}_1(t), \tag{A4}$$

$$\frac{d\vec{V}_2(t)}{dt} = \mathbf{M}_2 \vec{V}_2(t). \tag{A5}$$

Here, the vectors  $\vec{V}_1 = (\langle \hat{\sigma}_B^z \rangle, \langle \hat{\sigma}_C^z \rangle, \Re[\langle \hat{\sigma}_C^+ \hat{\sigma}_B^- \rangle], \Im[\langle \hat{\sigma}_C^+ \hat{\sigma}_B^- \rangle], \Re[\langle \hat{\sigma}_C^z \hat{\sigma}_B^- \rangle], \Im[\langle \hat{\sigma}_C^z \hat{\sigma}_B^- \rangle], \Re[\langle \hat{\sigma}_C^- \hat{\sigma}_B^- \rangle], \Im[\langle \hat{\sigma}_C^- \hat{\sigma}_B^- \rangle], \Re[\langle \hat{\sigma}_C^- \rangle], \Im[\langle \hat{\sigma}_C^- \rangle])^T$  and  $\vec{V}_2 = (\Re[\langle \hat{\sigma}_B^- \rangle], \Im[\langle \hat{\sigma}_B^- \rangle], \Re[\langle \hat{\sigma}_C^- \hat{\sigma}_B^z \rangle], \Im[\langle \hat{\sigma}_C^- \hat{\sigma}_B^z \rangle], \langle \hat{\sigma}_C^z \hat{\sigma}_B^z \rangle)^T$  and  $\mathbf{M}_1, \mathbf{M}_2$  are  $10 \times 10, 5 \times 5$  (respectively) matrices that can be read off from Eqs. (A1) and (A2).

### 1. Resonant Case — Analytical Solution

Considering the resonant limit with  $\Delta_{CB} = \Delta_{Cd} = 0$ , Eqs. (A4) and (A5), with the initial condition  $\vec{V}_1(0) = (-1 \ -1 \ 0 \ 0 \ 0 \ 0 \ 0 \ 0 \ 0 \ 0)^T, \vec{V}_2(0) = (0 \ 0 \ 0 \ 0 \ 1)^T$ , can be solved by taking the Laplace transform  $\mathcal{L}[\vec{V}_i(t)] = \int_0^\infty dt e^{-st} \vec{V}_i(t)$  on both sides to obtain,

$$\mathcal{L}[\vec{V}_i(t)] = \frac{1}{(s\mathcal{I} - \mathbf{M}_i)^{-1}} \vec{V}_i(0), \tag{A6}$$

with  $i = 1, 2$ . From the inverse Laplace transform of the above relation we immediately obtain the following

expressions for  $\langle \hat{\sigma}_B^z \rangle$ ,  $\langle \hat{\sigma}_B^+ \rangle$ , which are the variables of interest to compute the energy and ergotropy:

$$\begin{aligned} \langle \hat{\sigma}_B^z \rangle(t) = & -\frac{e^{-\frac{\gamma_C}{4}t}}{2\left(1 + 4\frac{F^2}{g^2}\right)} \left\{ \frac{8F^2}{g^2} \chi_t(\gamma_C, g, f_0) \right. \\ & + \left(1 + \sqrt{1 + \frac{4F^2}{g^2}}\right) \chi_t(\gamma_C, g, f_1) \\ & \left. + \left(1 - \sqrt{1 + \frac{4F^2}{g^2}}\right) \chi_t(\gamma_C, g, f_2) \right\} \end{aligned} \quad (\text{A7})$$

with

$$\begin{aligned} \chi_t(\gamma_C, g, f_i) = & \left[ \cosh\left(\frac{\sqrt{\gamma_C^2 - 32f_i g^2}t}{4}\right) \right. \\ & \left. + \frac{\gamma_C}{\sqrt{\gamma_C^2 - 32f_i g^2}} \sinh\left(\frac{\sqrt{\gamma_C^2 - 32f_i g^2}t}{4}\right) \right], \end{aligned} \quad (\text{A8})$$

$f_0 = 1/2$ ,  $f_1 = \left(1 + 2F^2/g^2 - \sqrt{1 + 4F^2/g^2}\right)$  and  $f_2 = \left(1 + 2F^2/g^2 + \sqrt{1 + 4F^2/g^2}\right)$ , and

$$\begin{aligned} \langle \hat{\sigma}_B^- \rangle(t) = & \frac{-\frac{F}{g}}{1 + \frac{4F^2}{g^2}} + e^{-\frac{\gamma_C}{4}t} \left\{ \cosh\left[\frac{\sqrt{\gamma_C^2 - 16(g^2 + 4F^2)}t}{4}\right] \right. \\ & \left. + \frac{\gamma_C}{\sqrt{\gamma_C^2 - 16(g^2 + 4F^2)}} \sinh\left[\frac{t}{4}\sqrt{\gamma_C^2 - 16(g^2 + 4F^2)}\right] \right\}. \end{aligned} \quad (\text{A9})$$

From Eqs. (A7) and (A9), we can write down the exact expressions for the average energy  $E_B(t)$  and ergotropy  $\mathcal{E}_B(t)$  of the battery. The average energy is given by,

$$\begin{aligned} \frac{E_B(t)}{\omega_B} = & \frac{1}{2} - \frac{e^{-\frac{\gamma_C}{4}t}}{4\left(1 + 4\frac{F^2}{g^2}\right)} \left\{ \frac{8F^2}{g^2} \chi_t(\gamma_C, g, f_0) \right. \\ & + \left(1 + \sqrt{1 + \frac{4F^2}{g^2}}\right) \chi_t(\gamma_C, g, f_1) \\ & \left. + \left(1 - \sqrt{1 + \frac{4F^2}{g^2}}\right) \chi_t(\gamma_C, g, f_2) \right\}. \end{aligned} \quad (\text{A10})$$

The exact analytical expression for ergotropy is cumbersome and we do not present it here for brevity. Nonetheless, we have evaluated this expression and plotted the results for weak driving in Fig. 2(b) and in Fig. 12 (a,b) for moderate and strong driving respectively. Let us now consider the steady-state solution of Eqs. (A4) and (A5). For the resonant case, we have that

$$\begin{aligned} \det(\mathbf{M}_1) &= 4F^4 g^2 \gamma_C^2 (2F^2 + g^2), \\ \det(\mathbf{M}_2) &= 0. \end{aligned}$$

Thus the steady-state solution for  $\vec{V}_1(t \rightarrow \infty) = \vec{V}_1^{\text{ss}} = 0$ . This implies  $\langle \hat{\sigma}_B^z \rangle(t \rightarrow \infty) = 0$ , and hence we have

$$E_B(t \rightarrow \infty) = \frac{\omega_B}{2}. \quad (\text{A11})$$

Since the determinant of  $\mathbf{M}_2$  is zero, the variables in  $\vec{V}_2$  do not have a unique steady state. Nonetheless, we can take the long-time limit of the solutions with the initial conditions in question. To this end since the ergotropy Eq. (10) depends on  $\langle \hat{\sigma}_B^- \rangle$  in addition  $\langle \hat{\sigma}_B^z \rangle$ , from Eq. (A9) we have that  $\langle \hat{\sigma}_B^- \rangle(t \rightarrow \infty) = \frac{-F/g}{1 + 4F^2/g^2}$  leading to:

$$\mathcal{E}_B(t \rightarrow \infty) = \frac{F/g}{1 + 4F^2/g^2} \omega_B. \quad (\text{A12})$$

As we remarked in the main text, instead of a single battery we can also consider the scenario of multiple identical batteries (say  $N$ ) coupled in a star configuration (collective coupling) to a single charger. In this case, the only change is in the Hamiltonian Eq. (5) which becomes

$$\begin{aligned} \hat{H} = & \omega_C \hat{\sigma}_C^+ \hat{\sigma}_C^- + \omega_B \sum_{j=1}^N \hat{\sigma}_{B,j}^+ \hat{\sigma}_{B,j}^- + g \left( \hat{\sigma}_C^+ \sum_{j=1}^N \hat{\sigma}_{B,j}^- + \text{h.c.} \right) \\ & + F(\hat{\sigma}_C^- e^{i\omega_C t} + \hat{\sigma}_C^+ e^{-i\omega_C t}) \end{aligned} \quad (\text{A13})$$

with h.c. denoting the hermitian conjugate. With this change, as displayed in Fig. 13, we see that the ratio of the steady-state ergotropy to the energy can be made larger by increasing  $N$ . More precisely, we find this ratio to be 0.5, 0.62, 0.69 for  $N = 1, 2, 3$  respectively. Corresponding values of the optimal driving strength to coupling ratios  $F/g$  are given 0.5, 0.73, 0.94. In a forthcoming work [52], we will explore in detail the charging dynamics and other features of the set-up with multiple batteries.

## 2. Resonant Case — Charging Time Analysis

Let us now provide the details justifying the charging time analysis leading to Eqs. (17) and (19) in the main text. To this end, let us first consider the limit of  $\gamma_C \ll g$  in the energy expression Eq. (A10). It is immediately clear that in this limit all the hyperbolic trigonometric functions will become standard trigonometric functions and the function  $\chi$  in Eq. (A10) becomes

$$\chi(\gamma_C, g, f_j) \stackrel{\gamma_C \ll g}{\approx} \cos(\sqrt{2f_j}gt) + \frac{\frac{\gamma_C}{g}}{\sqrt{32f_j}} \sin(\sqrt{2f_j}gt)$$

with  $j = 0, 1, 2$ . This leads to

$$\left| \frac{E_B(\tau) - E_B(t \rightarrow \infty)}{E_B(0) - E_B(t \rightarrow \infty)} \right| = e^{-\frac{\gamma_C}{4}t} \phi(F, g, \gamma_C, \tau), \quad (\text{A14})$$

$$\begin{aligned} \phi(F, g, \gamma_C, \tau) = & \frac{1}{2(1 + \frac{F^2}{g^2})} \left\{ \frac{8F^2}{g^2} \left[ \cos(g\tau) + \frac{\gamma_C}{4g} \sin(g\tau) \right] \right. \\ & + \left( 1 + \sqrt{1 + \frac{4F^2}{g^2}} \right) \\ & \left[ \cos(\sqrt{2f_1}g\tau) + \frac{\gamma_C}{\sqrt{32f_1}} \sin(\sqrt{2f_1}g\tau) \right] \\ & + \left( 1 - \sqrt{1 + \frac{4F^2}{g^2}} \right) \\ & \left. \times \left[ \cos(\sqrt{2f_2}g\tau) + \frac{\gamma_C}{\sqrt{32f_2}} \sin(\sqrt{2f_2}g\tau) \right] \right\}, \quad (\text{A15}) \end{aligned}$$

justifying the expressions in Eq. (17) in the main text.

Considering now the opposite limit of  $\gamma_C \gg \{F, g\}$ , we can make the approximations

$$\begin{aligned} 2\chi(\gamma_C, g, f_j) & \stackrel{\gamma_C \gg \{F, g\}}{\approx} e^{-\frac{4g^2 f_j t}{\gamma_C}} + e^{-\frac{\gamma_C t}{2}} e^{\frac{4g^2 f_j t}{\gamma_C}} \\ & + \left( 1 + \frac{16f_j g^2}{\gamma_C^2} \right) \left( e^{-\frac{4g^2 f_j t}{\gamma_C}} - e^{-\frac{\gamma_C t}{2}} e^{\frac{4g^2 f_j t}{\gamma_C}} \right). \end{aligned}$$

Substituting this into Eq. (A10) and keeping terms to order  $\frac{1}{\gamma_C}$ , we will immediately be lead to Eq. (19) in the main text.

Let us now briefly analyze the large and small driving limit of Eq. (19). In the large driving limit with  $F/g \gg 1$ , we have  $f_1 = 1 - \frac{2F}{g} + 2\frac{F^2}{g^2} + O(g/F)$  and  $f_2 = 1 + \frac{2F}{g} + 2\frac{F^2}{g^2} + O(g/F)$ . Thus, we have the inequality

$$\frac{f_2 g^2}{\gamma_C} > \frac{f_1 g^2}{\gamma_C} > \frac{2g^2}{\gamma_C},$$

which leads to the conclusion that the slowest damping scale that sets the charging time is precisely given by  $\frac{2g^2}{\gamma_C}$ . In the weak driving limit of  $F/g \ll 1$ , we have  $f_1 = 2\frac{F^4}{g^4} + O(F^6/g^6)$  and  $f_2 = 2 + 4\frac{F^2}{g^2} + O(F^4/g^4)$ , and the inequality

$$\frac{f_2 g^2}{\gamma_C} > \frac{2g^2}{\gamma_C} > \frac{f_1 g^2}{\gamma_C}$$

which leads to the conclusion that the slowest damping scale that sets the charging time is precisely given by  $\frac{f_1 g^2}{\gamma_C}$ . This simplifies the solution for the charging time Eq. (19) to

$$\frac{1 + \sqrt{1 + \frac{4F^2}{g^2}}}{2 \left( 1 + \frac{4F^2}{g^2} \right)} e^{-\frac{4f_1 g^2}{\gamma_C} \tau} = e^{-n}.$$

Taking the logarithm and expanding the left-hand side to lowest order in  $F/g$ , which turns out to be  $g^4/F^4$ , we find the result  $\tau = \frac{ng^2}{F^4} \gamma_C$  which is given as Eq. (20) in the main text.

We finish our consideration of the resonant case by estimating the optimal dephasing  $\gamma_C^*$  by identifying the underdamped to the overdamped transition of the exact expression of the average energy  $E_B(t)$  in Eq. (A10). Let us first consider the limit of small driving  $F/g \ll 1$ . In the limit  $F/g \ll 1$ , comparing the relative amplitude of the three contributing terms, it becomes immediately clear that the largest amplitude term is the one with  $1 + \sqrt{1 + 4\frac{F^2}{g^2}} \approx 2$ . Looking at the dynamical part of this term, it has an underdamped to overdamped transition when  $\gamma_C^2 = 32f_1$ . Also in the limit of small  $F/g \ll 1$ ,  $f_1 \approx 2\frac{F^4}{g^4}$ , thus we have the estimate of the first transition as,

$$\gamma_C^* \stackrel{F \ll g}{\approx} \frac{8F^2}{g}. \quad (\text{A16})$$

For large  $F/g \gg 1$  case, since  $8F^2/g^2/(1 + 4F^2/g^2) \approx 2$  is much larger than  $(1 \pm \sqrt{1 + 4F^2/g^2})/(1 + 4F^2/g^2) \approx \pm 1/\sqrt{1 + 4F^2/g^2}$ , the first term is the one with the largest magnitude and it has an underdamped to overdamped transition precisely at,

$$\gamma_C^* \sim 4g. \quad (\text{A17})$$

Note that the above expressions for optimal dephasing agree qualitatively with the ones given in the main text in Eqs. (22) and (23).

### 3. Detuned Case — Steady State

While in principle we can solve the equations of motion (A4) and (A5) for the scenario where the detunings  $\Delta_{\text{Bd}}$  and/or  $\Delta_{\text{Cd}}$  are non-zero, we find that in general the expressions for these solutions are unwieldy and do not add more insight for both with and without dephasing  $\gamma_C$ . Nevertheless, as we comment below, we can make some strong statements regarding the long-time or steady-state behavior of the figures of merit in this case (with  $\gamma_C \neq 0$ ). To this end, for the case of the battery and charger resonant with each other but detuned from the drive, i.e.,  $\Delta_{\text{Bd}} = \Delta_{\text{Cd}} \neq 0$ , we have that the determinants of  $\mathbf{M}_i$ ,

$$\begin{aligned} \det(\mathbf{M}_1) &= \frac{F^2 g^2 \gamma_C}{2} (16F^4(\gamma_C - 4\Delta_{\text{Cd}}) + 4F^2(2g^2 \gamma_C \\ &+ (\gamma_C - 4\Delta_{\text{Cd}})^2 \Delta_{\text{Cd}}) + \gamma_C \Delta_{\text{Cd}}^2 (\gamma_C^2 + 16\Delta_{\text{Cd}}^2)), \\ \det(\mathbf{M}_2) &= -2F^2 \gamma_C \Delta_{\text{Cd}}^2, \end{aligned}$$

are non-zero. As a result, the steady solutions are given by  $\vec{V}_1 = \vec{V}_2 = 0$ . This immediately means that for this case, we have the steady-state energy and ergotropy take

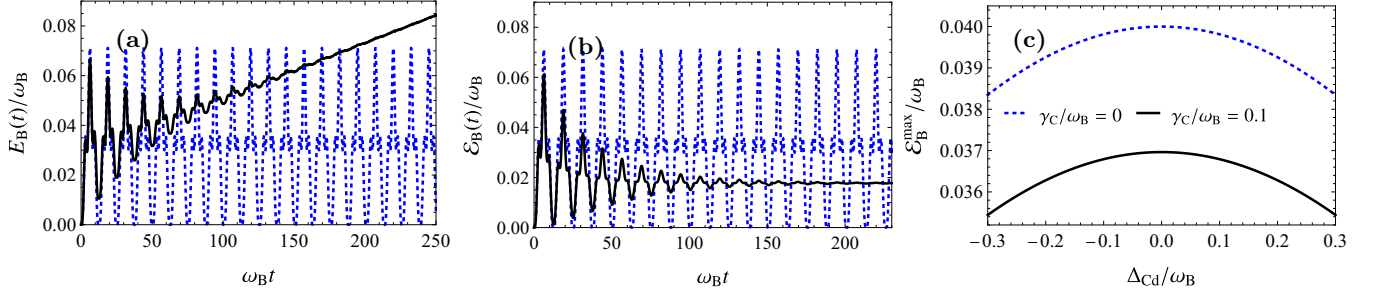


FIG. 14. (Color Online) Transient dynamics of the average energy  $E_B(t)$  (a) and ergotropy  $\mathcal{E}_B(t)$  (b) of the battery for two-HO model in the weak driving regime  $F/g = 0.1$  for the detuned driving  $\Delta_{Cd} = \Delta_{Bd} = 0.5$ . Maximum value of ergotropy  $\mathcal{E}_B^{\max}(c)$  as a function of drive detuning  $\Delta_{Cd} = \Delta_{Bd}$ . Other parameters are  $F = 0.1\omega_B$  and  $g = 1.0\omega_B$ .

the values

$$\begin{aligned} E_B(t \rightarrow \infty) &= \frac{\omega_B}{2}, \\ \mathcal{E}_B(t \rightarrow \infty) &= 0, \end{aligned}$$

as we mentioned in the main text. In contrast, for the alternate detuning scenario with  $\Delta_{CB} = \Delta_{Cd} \neq 0$  and  $\Delta_{Bd} = 0$ , we have that:

$$\begin{aligned} \det(\mathbf{M}_1) &= 4F^4 g^2 \gamma_C (g^2 \gamma_C + 2F^2 (\gamma_C - 2\Delta_{CB})) \\ \det(\mathbf{M}_2) &= 0. \end{aligned}$$

Thus as before while this leads to  $\vec{V}_1 = 0$ ,  $\langle \hat{\sigma}_z \rangle(t \rightarrow \infty) = 0$  and steady-state energy of  $E_B(t \rightarrow \infty) = \omega_B/2$ , the steady-state value of ergotropy has to be determined by calculating  $\langle \hat{\sigma}_B^- \rangle(t)$  and taking the long-time limit. When we do this, we find that interestingly the ergotropy is given by

$$\mathcal{E}_B(t \rightarrow \infty) = \frac{F/g}{1 + 4F^2/g^2} \omega_B, \quad (\text{A18})$$

which is the same result that we found in the resonant case.

## Appendix B: Two-HO Model

In this appendix, we discuss additional details corresponding to the two-HO model of the charger battery system. As with the TLS case, to discuss the analytical solutions for the two-HO model with detuning, it is convenient to work in a frame that is transformed with respect to the original master equation (2) via the unitary  $\hat{U} = e^{i\omega_d(\hat{a}_C^\dagger \hat{a}_C + \hat{a}_B^\dagger \hat{a}_B)t}$ . With this approach, the two-HO Hamiltonian in the frame rotating at the drive frequency reads

$$\begin{aligned} \hat{H} &= \Delta_{Cd} \hat{a}_C^\dagger \hat{a}_C + \Delta_{Bd} \hat{a}_B^\dagger \hat{a}_B + g (\hat{a}_C^\dagger \hat{a}_B + \hat{a}_B^\dagger \hat{a}_C) \\ &+ F(\hat{a}_C + \hat{a}_C^\dagger), \end{aligned} \quad (\text{B1})$$

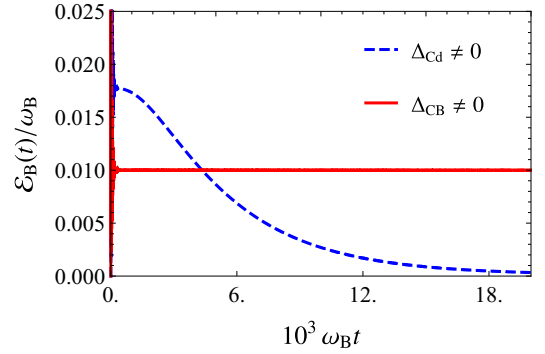


FIG. 15. (Color Online) Time evolution of the ergotropy of two-HO model for the detuned driving ( $\Delta_{Bd} = \Delta_{Cd} = 0.5\omega_B$ ) and the detuned charger ( $\Delta_{Bd} = 0$  and  $\Delta_{CB} = 0.5\omega_B$ ). Other parameter values are  $F = 0.1\omega_B$ ,  $g = 1.0\omega_B$ ,  $\gamma_C = 0.1\omega_B$ .

with the detunings as defined in the TLS case. The master equation in this transformed frame leads to the following equations for the operator expectation values:

$$\begin{aligned} \frac{d}{dt} \langle \hat{a}_B^\dagger \hat{a}_B \rangle &= -2g \Im \mathbf{m} [\langle \hat{a}_C^\dagger \hat{a}_B \rangle] \\ \frac{d}{dt} \langle \hat{a}_C^\dagger \hat{a}_C \rangle &= -2F \Im \mathbf{m} [\langle \hat{a}_C \rangle] + 2g \Im \mathbf{m} [\langle \hat{a}_C^\dagger \hat{a}_B \rangle] \\ \frac{d}{dt} \langle \hat{a}_C^\dagger \hat{a}_B \rangle &= iF \langle \hat{a}_B \rangle - ig (\langle \hat{a}_C^\dagger \hat{a}_C \rangle - \langle \hat{a}_B^\dagger \hat{a}_B \rangle) \\ &\quad - \left[ \frac{\gamma_C}{2} - i(\Delta_{Cd} - \Delta_{Bd}) \right] \langle \hat{a}_C^\dagger \hat{a}_B \rangle \\ \frac{d}{dt} \langle \hat{a}_B \rangle &= -ig \langle \hat{a}_C \rangle - i\Delta_{Bd} \langle \hat{a}_B \rangle \\ \frac{d}{dt} \langle \hat{a}_C \rangle &= -iF - ig \langle \hat{a}_B \rangle - \left( \frac{\gamma_C}{2} + i\Delta_{Cd} \right) \langle \hat{a}_C \rangle. \end{aligned} \quad (\text{B2})$$

As described in the main text, while the solution of the above equations of motion can help us calculate the average energy of the battery, we have to solve the master equation numerically to determine the ergotropy with non-zero dephasing. Similar to the TLS case, we collect the equations for the expectation values into a matrix

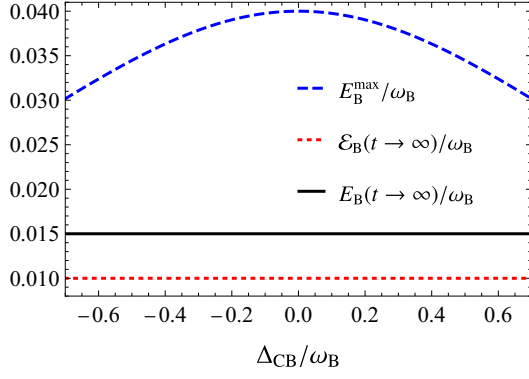


FIG. 16. (Color Online) Comparison of the maximum value of the average energy and ergotropy  $E_B^{\max}/\omega_B = \mathcal{E}_B^{\max}/\omega_B$  of two-HO model for the zero dephasing  $\gamma_C = 0$  and the long-time steady state values of average energy (red dashed line) and ergotropy (black dot-dashed line) for non-zero dephasing  $\gamma_C = 0.1\omega_B$ .

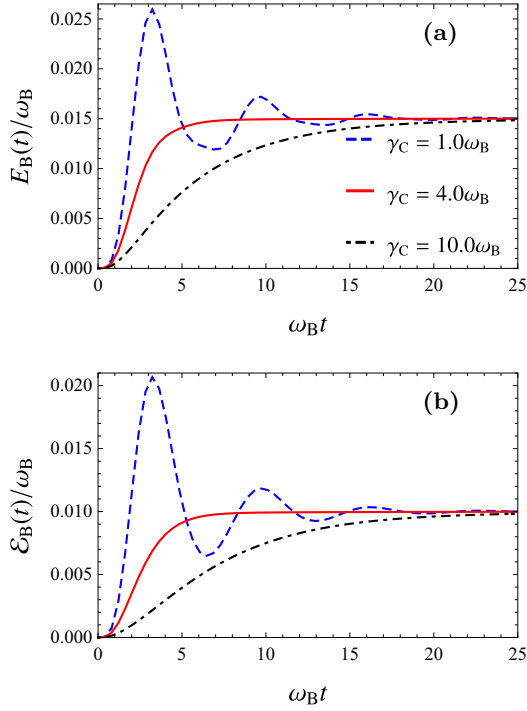


FIG. 17. (Color Online) Time evolution of average energy  $E_B(t)$ (a) and ergotropy  $\mathcal{E}_B(t)$ (b) of the battery for the TLS-HO model for the weak driving case  $F = 0.1\omega_B, g = \omega_B$  ( $F/g = 0.1$ ) for different values of the dephasing rate  $\gamma_C$ . Other parameter values are  $\omega_C = \omega_d = \omega_B$ .

form as,

$$\frac{d\vec{V}(t)}{dt} = \mathbf{M}\vec{V}(t) + \vec{W}, \quad (\text{B3})$$

where the vectors  $\vec{V} = (\langle \hat{a}_B^\dagger \hat{a}_B \rangle, \langle \hat{a}_C^\dagger \hat{a}_C \rangle, \Im[\langle \hat{a}_C^\dagger \hat{a}_B \rangle], \Re[\langle \hat{a}_C^\dagger \hat{a}_B \rangle], \Re[\hat{a}_B], \Im[\hat{a}_B], \Re[\hat{a}_C], \Im[\hat{a}_C])^T$

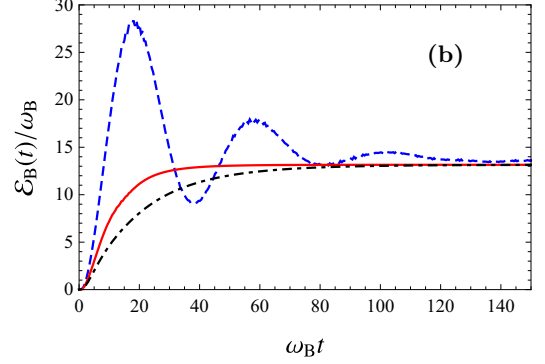
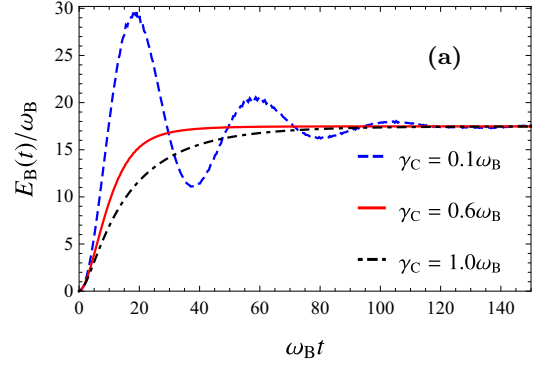


FIG. 18. (Color Online) Time evolution of average energy  $E_B(t)$ (a) and ergotropy  $\mathcal{E}_B(t)$ (b) of the battery for the TLS-HO model for the strong driving case  $F = 3.0\omega_B, g = \omega_B$  ( $F/g = 3.0$ ) for different values of the dephasing rate  $\gamma_C$  for the resonant case, i.e.,  $\omega_C = \omega_d = \omega_B$ .

and  $\vec{W} = (0, 0, 0, 0, 0, 0, 0, -F)^T$  with  $\mathbf{M}$  is a  $8 \times 8$  matrix which can be read off from Eq. (B2) after separating the real and imaginary parts. Note in contrast to the two-TLS model, the EOMs are inhomogeneous. The density matrix at initial time  $\hat{\rho}'(t=0) = |0\rangle\langle 0|_B \otimes |0\rangle\langle 0|_C$  translates to the initial condition  $\vec{V}(0) = (0, 0, 0, 0, 0, 0, 0, 0)^T$ . By taking the Laplace transform  $\mathcal{L}[\vec{V}(t)] = \int_0^\infty dt e^{-st} \vec{V}(t)$  on both sides of Eq. (B3), we obtain

$$\mathcal{L}[\vec{V}(t)] = \frac{1}{s(s\mathbf{I} - \mathbf{M})^{-1}} \vec{W}. \quad (\text{B4})$$

By taking the inverse Laplace transform of the above equation, we can determine  $\langle \hat{a}_B^\dagger \hat{a}_B \rangle(t)$ .

Since we have provided the results for the resonant scenario in the main text, in this appendix we will consider the situation with finite detuning. Focusing first on the zero dephasing case, we note that Eq. (B2) can be solved to obtain tractable analytical expressions. As discussed in [27], for the closed gaussian dynamics of the oscillators the energy and ergotropy coincide for our choice of initial conditions. Let us first look at the case of detuned driving with  $(\Delta_{Bd} = \Delta_{Cd}) \neq 0$ . By solving the equations of motion Eq. (B2) with non-zero detuning for the closed

case, the average energy takes the form

$$\frac{E_B(t)}{\omega_B} = \frac{F^2}{2(\Delta_{Cd}^2 - g^2)^2} [3g^2 + g^2 \cos(2gt) - 4g^2 \cos(gt) \cos(\Delta_{Cd}t) + 2\sin(gt)\Delta_{Cd}(\Delta_{Cd} \sin(gt) - 2g \sin(\Delta_{Cd}t))]. \quad (\text{B5})$$

This purely oscillatory evolution, depicted for an exemplary parameter choice in Figs. 14(a) and 14(b), for  $\Delta_{Cd} < g$  takes its maximum amplitude of

$$\frac{E_B^{\text{Max}}}{\omega_B} = \frac{4F^2 g^2}{(\Delta_{Cd}^2 - g^2)^2} \cos^2\left(\frac{\Delta_{Cd}\pi}{2g}\right), \quad (\text{B6})$$

at  $t = (2n+1)\pi/g$ . From Eqs. (B5) and (B6), we can see that as  $\Delta_{Cd} \rightarrow \pm g$ , there is a resonant enhancement of the battery energy with an unbounded increase of energy and ergotropy. This is expected as the normal mode frequency of the coupled battery and charger (at resonance with each other) is precisely at  $\omega_B \pm g$  [41]. Coming to the case where the battery and charger are detuned, i.e.  $\Delta_{Bd} = 0$  and  $\Delta_{CB} \neq 0$ , the energy is given by

$$\begin{aligned} \frac{E_B(t)}{\omega_B} = \frac{F^2}{g^2} & \left\{ 2 - \frac{2g^2}{\Delta_{CB}^2 + 4g^2} \right. \\ & + \frac{2g^2 \cos\left[\sqrt{\Delta_{CB}^2 + 4g^2}t\right]}{\Delta_{CB}^2 + 4g^2} - \left[ \cos\left(\frac{gt}{\alpha}\right) + \cos(\alpha t) \right] \\ & \left. - \frac{\Delta_{CB}}{\sqrt{\Delta_{CB}^2 + 4g^2}} \left[ \cos\left(\frac{gt}{\alpha}\right) - \cos(\alpha t) \right] \right\}, \quad (\text{B7}) \end{aligned}$$

where  $\alpha = \sqrt{g^2 + \frac{1}{2}\Delta_{CB}^2 + \frac{1}{2}\Delta_{CB}\sqrt{\Delta_{CB}^2 + 4g^2}}$ . A key point of difference with the above expression compared to Eq. (B5) is that it does not diverge at  $\Delta_{CB} = \pm g$ .

As in the TLS case, for the case with dephasing and non-zero detuning, analytical solutions for the energy become involved. Nonetheless, we can extract some key features of the dynamics at long times. Considering first the case of detuned driving with  $(\Delta_{Bd} = \Delta_{Cd}) \neq 0$ , we find that at long times the energy becomes a linear function of time of the form

$$\frac{E_B(t)}{\omega_B} \underset{\omega_B t \gg 1}{\approx} \frac{2F^2 \gamma_C \Delta_{Cd}^2 t}{4g^4 - 8g^2 \Delta_{Cd}^2 + \gamma_C^2 \Delta_{Cd}^2 + 4\Delta_{Cd}^4}, \quad (\text{B8})$$

as shown in Fig. 14(a). Thus, in contrast to the two-TLS model, looking at transient maxima of  $E_B(t)$  is not meaningful for the two-HO model for the detuned driving case. Coming to the ergotropy, which we calculate numerically using QuTIP [56], we see in Fig. 14(b) that after initial oscillations it settles to an intermediate value. Over much longer time scales, as shown in Fig. 15, we find that the ergotropy damps towards zero similar to the TLS case. Let us now compare the behavior of this transient maxima of the ergotropy in the case with dephasing to the closed case. As shown in Fig. 14(c), unlike

the TLS case, for  $|\Delta_{Cd}| < g$  with detunings close to resonance the ergotropy with dephasing is always smaller than the closed case. While we have depicted the behavior around  $\Delta_{Cd} = 0$  to better compare with the TLS results, the ergotropy in the dephased charger case also has peaks at  $\Delta_{Cd} = \pm g$ . Examining the case where the battery and charger are detuned ( $\Delta_{CB} \neq 0, \Delta_{Bd} = 0$ ), we find by taking the  $t \rightarrow \infty$  limit from an analytical solution of Eq. (B3) that the average energy becomes

$$\frac{E_B(t \rightarrow \infty)}{\omega_B} = \frac{3F^2}{2g^2}, \quad (\text{B9})$$

which is exactly equal to the steady state in the resonant case. Though we do not have analytical expression for the ergotropy, from a numerical solution of the master equation, as shown in Fig. 15, we find that while the ergotropy goes to zero in the long time limit for  $\Delta_{Bd} = \Delta_{Cd} \neq 0$ , it goes to a steady non-zero value for the case of  $\Delta_{CB} \neq 0$  and  $\Delta_{Bd} = 0$ . Moreover, we find by varying the ratio between the driving and coupling strength  $F/g$ , the long-time ergotropy for the latter case behaves as  $\frac{E_B(t \rightarrow \infty)}{\omega_B} = F^2/g^2$  agreeing with the result from the resonant case. Finally, we also see from Fig. 16 that even for the case of  $\Delta_{CB} \neq 0$  and  $\Delta_{Bd} = 0$ , for  $|\Delta_{CB}| < g$ , the steady state ergotropy in the non-zero dephasing case is smaller than the maximum value taken by the oscillating ergotropy in the closed case.

### Appendix C: TLS-HO Model

To illustrate the generality of the central results of our paper, we consider the scenario of a driven TLS charger connected to an HO battery with the Hamiltonian given by

$$\begin{aligned} \hat{H} = \omega_C \hat{\sigma}_C^+ \hat{\sigma}_C^- + \omega_B \hat{a}_B^\dagger \hat{a}_B + g(\hat{\sigma}_C^+ \hat{a}_B + \hat{\sigma}_C^- \hat{a}_B^\dagger) \\ + F(\hat{\sigma}_C^- e^{i\omega_a t} + \hat{\sigma}_C^+ e^{-i\omega_a t}). \quad (\text{C1}) \end{aligned}$$

The dynamics of interest, as before, is given by the master equation

$$\frac{d\hat{\rho}(t)}{dt} = -i \left[ \hat{H}, \hat{\rho}(t) \right] + \frac{\gamma_C}{4} (\hat{\sigma}_C^z \hat{\rho}(t) \hat{\sigma}_C^z - \hat{\rho}(t)). \quad (\text{C2})$$

Similar to the two-TLS and two-HO cases, we can derive equations of motion for the operator expectation values but for brevity, we numerically simulate the master equation (C2) [56], which is nothing but a driven version of the Jaynes-Cummings model. As shown in Figs. 17 and 18, we see that for both weak ( $F \ll g$ ) and strong driving ( $F \geq g$ ), there is an optimum dephasing rate at which fastest charging is achieved. Unsurprisingly, even though the battery is given by an HO system, in this case, due to the TLS charger, we have that the optimal dephasing is dependent on the strength of driving.

- 
- [1] J. Quach, G. Cerullo, and T. Virgili, *Joule* **7**, 2195 (2023).
- [2] S. Bhattacharjee and A. Dutta, *Eur. Phys. J. B* **94**, 239 (2021).
- [3] N. M. Myers, O. Abah, and S. Deffner, *AVS Quantum Sci.* **4**, 027101 (2022).
- [4] F. Campaioli, F. A. Pollock, and S. Vinjanampathy, Quantum batteries, in *Thermodynamics in the Quantum Regime: Fundamental Aspects and New Directions*, edited by F. Binder, L. A. Correa, C. Gogolin, J. Anders, and G. Adesso (Springer International Publishing, Cham, 2018) pp. 207–225.
- [5] G. M. Andolina, D. Farina, A. Mari, V. Pellegrini, V. Giovannetti, and M. Polini, *Phys. Rev. B* **98**, 205423 (2018).
- [6] L. P. García-Pintos, A. Hamma, and A. del Campo, *Phys. Rev. Lett.* **125**, 040601 (2020).
- [7] P. Chen, T. S. Yin, Z. Q. Jiang, and G. R. Jin, *Phys. Rev. E* **106**, 054119 (2022).
- [8] F.-Q. Dou, Y.-J. Wang, and J.-A. Sun, *Front. Phys.* **17**, 31503 (2021).
- [9] J.-Y. Gyhm, D. Rosa, and D. Šafránek, [arXiv:2308.16086](https://arxiv.org/abs/2308.16086) (2023), [arXiv:2308.16086](https://arxiv.org/abs/2308.16086) [quant-ph].
- [10] F. Campaioli, S. Gherardini, J. Q. Quach, M. Polini, and G. M. Andolina, [arXiv:2308.02277](https://arxiv.org/abs/2308.02277) (2023), [arXiv:2308.02277](https://arxiv.org/abs/2308.02277) [quant-ph].
- [11] R. Alicki and M. Fannes, *Phys. Rev. E* **87**, 042123 (2013).
- [12] K. V. Hovhannisyán, M. Perarnau-Llobet, M. Huber, and A. Acín, *Phys. Rev. Lett.* **111**, 240401 (2013).
- [13] F. C. Binder, S. Vinjanampathy, K. Modi, and J. Goold, *New J. Phys.* **17**, 075015 (2015).
- [14] F. Campaioli, F. A. Pollock, F. C. Binder, L. Céleri, J. Goold, S. Vinjanampathy, and K. Modi, *Phys. Rev. Lett.* **118**, 150601 (2017).
- [15] D. Ferraro, M. Campisi, G. M. Andolina, V. Pellegrini, and M. Polini, *Phys. Rev. Lett.* **120**, 117702 (2018).
- [16] G. M. Andolina, M. Keck, A. Mari, M. Campisi, V. Giovannetti, and M. Polini, *Phys. Rev. Lett.* **122**, 047702 (2019).
- [17] K. Ito and G. Watanabe, [arXiv:2008.07089](https://arxiv.org/abs/2008.07089) (2020), [arXiv:2008.07089](https://arxiv.org/abs/2008.07089) [quant-ph].
- [18] D. Rossini, G. M. Andolina, D. Rosa, M. Carrega, and M. Polini, *Phys. Rev. Lett.* **125**, 236402 (2020).
- [19] S. Julià-Farré, T. Salamon, A. Riera, M. N. Bera, and M. Lewenstein, *Phys. Rev. Res.* **2**, 023113 (2020).
- [20] G. Watanabe, B. P. Venkatesh, P. Talkner, M.-J. Hwang, and A. del Campo, *Phys. Rev. Lett.* **124**, 210603 (2020).
- [21] J.-Y. Gyhm, D. Šafránek, and D. Rosa, *Phys. Rev. Lett.* **128**, 140501 (2022).
- [22] J.-S. Yan and J. Jing, *Phys. Rev. Appl.* **19**, 064069 (2023).
- [23] D.-L. Yang, F.-M. Yang, and F.-Q. Dou, [arXiv:2308.01188](https://arxiv.org/abs/2308.01188) (2023), [arXiv:2308.01188](https://arxiv.org/abs/2308.01188) [quant-ph].
- [24] J. Liu, D. Segal, and G. Hanna, *The Journal of Physical Chemistry C* **123**, 18303 (2019).
- [25] F. Pirmoradian and K. Mølmer, *Phys. Rev. A* **100**, 043833 (2019).
- [26] F. Barra, *Phys. Rev. Lett.* **122**, 210601 (2019).
- [27] D. Farina, G. M. Andolina, A. Mari, M. Polini, and V. Giovannetti, *Phys. Rev. B* **99**, 035421 (2019).
- [28] J. Q. Quach and W. J. Munro, *Phys. Rev. Appl.* **14**, 024092 (2020).
- [29] F. T. Tabesh, F. H. Kamin, and S. Salimi, *Phys. Rev. A* **102**, 052223 (2020).
- [30] F. H. Kamin, F. T. Tabesh, S. Salimi, F. Kheirandish, and A. C. Santos, *New Journal of Physics* **22**, 083007 (2020).
- [31] K. Xu, H.-J. Zhu, G.-F. Zhang, and W.-M. Liu, *Phys. Rev. E* **104**, 064143 (2021).
- [32] A. C. Santos, *Phys. Rev. E* **103**, 042118 (2021).
- [33] S. Ghosh, T. Chanda, S. Mal, and A. Sen(De), *Phys. Rev. A* **104**, 032207 (2021).
- [34] J. Q. Quach, K. E. McGhee, L. Ganzer, D. M. Rouse, B. W. Lovett, E. M. Gauger, J. Keeling, G. Cerullo, D. G. Lidzey, and T. Virgili, *Sci. Adv.* **8**, eabk3160 (2022), <https://www.science.org/doi/pdf/10.1126/sciadv.abk3160>.
- [35] F. Mayo and A. J. Roncaglia, *Phys. Rev. A* **105**, 062203 (2022).
- [36] R. R. Rodríguez, B. Ahmadi, G. Suarez, P. Mazurek, S. Barzanjeh, and P. Horodecki, [arXiv:2207.00094](https://arxiv.org/abs/2207.00094) (2023), [arXiv:2207.00094](https://arxiv.org/abs/2207.00094) [quant-ph].
- [37] F.-M. Yang and F.-Q. Dou, [arXiv:2312.11006](https://arxiv.org/abs/2312.11006) (2023), [arXiv:2312.11006](https://arxiv.org/abs/2312.11006) [quant-ph].
- [38] R. R. Rodríguez, B. Ahmadi, P. Mazurek, S. Barzanjeh, R. Alicki, and P. Horodecki, *Phys. Rev. A* **107**, 042419 (2023).
- [39] F.-Q. Dou and F.-M. Yang, *Phys. Rev. A* **107**, 023725 (2023).
- [40] B. Ahmadi, P. Mazurek, P. Horodecki, and S. Barzanjeh, [arXiv:2401.05090](https://arxiv.org/abs/2401.05090) (2024), [arXiv:2401.05090](https://arxiv.org/abs/2401.05090) [quant-ph].
- [41] K. Gangwar and A. Pathak, [arXiv:2401.07238](https://arxiv.org/abs/2401.07238) (2024), [arXiv:2401.07238](https://arxiv.org/abs/2401.07238) [quant-ph].
- [42] S. Diehl, A. Micheli, A. Kantian, B. Kraus, H. P. Büchler, and P. Zoller, *Nat. Phys.* **4**, 878 (2008).
- [43] B. Kraus, H. P. Büchler, S. Diehl, A. Kantian, A. Micheli, and P. Zoller, *Phys. Rev. A* **78**, 042307 (2008).
- [44] F. Verstraete, M. M. Wolf, and J. Ignacio Cirac, *Nat. Phys.* **5**, 633 (2009).
- [45] S. Gherardini, F. Campaioli, F. Caruso, and F. C. Binder, *Phys. Rev. Res.* **2**, 013095 (2020).
- [46] M. A. Nielsen and I. L. Chuang, *Quantum computation and quantum information* (Cambridge University Press, Cambridge, 2010).
- [47] J. L. Skinner and D. Hsu, *J. Phys. Chem.* **90**, 4931 (1986).
- [48] D. A. Lidar, Z. Bihary, and K. Whaley, *Chem. Phys.* **268**, 35 (2001).
- [49] T. Albash and D. A. Lidar, *Phys. Rev. A* **91**, 062320 (2015).
- [50] H. M. Wiseman and G. J. Milburn, *Quantum measurement and control* (Cambridge University Press, Cambridge, 2009).
- [51] J. Joshi and T. S. Mahesh, *Phys. Rev. A* **106**, 042601 (2022).
- [52] R. Shastri, C. Jiang, G.-H. Xu, B. Prasanna Venkatesh, and G. Watanabe, (unpublished).
- [53] G. Francica, F. C. Binder, G. Guarnieri, M. T. Mitchison, J. Goold, and F. Plastina, *Phys. Rev. Lett.* **125**, 180603 (2020).
- [54] C.-K. Hu, J. Qiu, P. J. P. Souza, J. Yuan, Y. Zhou, L. Zhang, J. Chu, X. Pan, L. Hu, J. Li, Y. Xu, Y. Zhong, S. Liu, F. Yan, D. Tan, R. Bachelard, C. J. Villas-Boas,

- A. C. Santos, and D. Yu, [Quantum Science and Technology](#) **7**, 045018 (2022).
- [55] S. Berger, M. Pechal, P. Kurpiers, A. A. Abdumalikov, C. Eichler, J. A. Mlynek, A. Shnirman, Y. Gefen, A. Wallraff, and S. Filipp, [Nat. Commun.](#) **6**, 8757 (2015).
- [56] J. Johansson, P. Nation, and F. Nori, [Comput. Phys. Commun.](#) **184**, 1234 (2013).